MASTER THESIS

Analysis of the Electric Fields of Lightning Discharge in the Same and in Different Channel

Submitted at the
Faculty of Electrical Engineering and Information Technology,
Vienna University of Technology
in partial fulfillment of the requirements for the degree of
Diplom-Ingenieur (equals Master of Science)

Under the supervision of

Univ.-Prof Dr.-Ing Wolfgang Gawlik
E370 Institute of Energy Systems and Electrical Drives

Dipl.Ing.Dr. Wolfgang Schulz
ÖVE, ALDIS

by

Shahed Hossain Syed Mahmud
Student ID number 9727178
Lorenz Böhler Gasse-4/3/4
1200 Vienna

January 7, 2019

_____

Kurzfassung

Das Phänomen „Gewitter und Blitze“ hatte Menschen immer beschäftigt. Neben menschlichem und tierischem Leben gehen auch wirtschaftliche Schäden wie Missernten, Haus- und Feuerbrände auf die Rechnung von Blitzen. Die elektromagnetischen Felder, welche von Blitzströmen hervorgerufen werden, erzeugen transiente Fehler in Hochspannungsleitungen und in manchen Fällen führen sie auch zum Ausfall von Hochspannungsnetzen. Aufgrund des großen Umfangs der Kumulonimbus-Wolke von ca. 10 bis 20 km ist es weder leicht, den Einschlagort eines Blitzes genau vorherzusagen, noch die ganze Fläche mit einem Blitzableiter zu schützen. Daher ist es wichtig, die Parameter, die einen Blitzeinschlag bedingen genau zu erforschen.

Umso mehr Blitzparameter wir kennen, desto effizienter können wir uns vor Blitzen schützen und das Ausmaß des Schadens verringern. Verschiedene Arten von Blitzen und deren Auftreten zu bestimmten Orten und Jahreszeiten, sowie deren Ursachen, werden von Blitzforschungsinstituten weltweit erforscht. Neben der Blitz-Charakteristik sind auch Faktoren wie Blitzstrom-Parameter, elektrische und elektromagnetische Felder sowie Orte mit hoher Blitzdichte von Forschungsinteresse. Die Untersuchung der Verteilung von Blitzdichten über unterschiedlichen Gebieten (Wohngebiete, Berge, Täler, Wald, Ackerland, etc.) und Blitzschlag an Windturbinen sind ebenso bedeutsam für verschiedenen Anwendungen, wie die Risikoanalyse, Klimaforschung, etc. So hat das Blitzortungssystem ALDIS in Österreich einige Orte mit hoher Blitzdichte aufgedeckt. Außerdem, stellte ALDIS fest, dass Berge und hohe Türme einen Trigger-Effekt für Blitze haben. Nieder gelegene Gebiete weisen hingegen wesentlich geringere Effekte auf.

In dieser Masterthesis wird die Hypothese untersucht, dass elektrische Felder von Haupt- und Folgeblitzen in dem gleichen Kanal eines negativen Wolke-Erde Blitzes einander mehr ähneln als die Haupt- und Folgeblitze vom benachbarten Kanal. Es wurde ein Excel Datenblatt mit elektrischen Felddaten von 74 Blitzen, die insgesamt 319 Haupt- und Folgeblitze enthalten, zur Verfügung gestellt. Die Videoaufzeichnungen von diesen Blitzen wurden ebenso bereitgestellt. Das Excel Datenblatt diente der schnellen Orientierung und als Referenz während der Analyse der Blitze. Für die Aufbereitung von Blitzdaten und die Anwendung von statistischen Methoden auf die Blitzdaten wurden Skriptprogramme in der Analysesoftware SCILAB implementiert. Um die Präzession der implementierten Funktionen zu überprüfen, wurden danach die elektrischen Felder der Blitze aus der implementierten Funktion geplottet und mit den, vom DataViewer geplotteten Diagrammen, verglichen. Da die elektrischen Felder mancher Blitze den Kriterien unserer Auswertungsmethodik nicht entsprachen, wurden diese verworfen. Die Felddaten wurden mittels Chi Quadrat und Kreuzkorrelation ausgewertet. Dabei wurden sowohl die Hauptblitze der benachbarten Kanäle desselben Blitzes miteinander als auch die Folgeblitze von benachbarten Kanälen desselben Blitzes miteinander vergleichen. Darüber hinaus wurden die Hauptblitze eines Blitzkanals mit den Folgeblitzen desselben Kanals miteinander und die Folgeblitze desselben Kanals miteinander verglichen. Schließlich wurden Mittelwerte von den Ergebnissen aus Chi Quadrat und Kreuzkorrelation gebildet und mit der Hypothese dieser Diplomarbeit verglichen.

Abstract

The phenomenon of lightning and thunder has drawn the attention of human beings for billions of years. Besides the loss of human and animal lives, also economic damages like crop failure, house and forest fires are caused by lightning. Further, the electromagnetic field generated by the lightning current frequently causes transient faults and blackouts in power transmission grids. Because of the large horizontal extent of a cumulonimbus cloud, which ranges from 10 to 20 km, it is not easy to predict the striking point precisely and it is not possible to prevent the whole area from being struck by lightning using a lightning rod.

The more lightning parameters we understand, the more efficiently we can take precautions against lightning damages. The lightning research institutes all over the world investigate the ratio of cloud to cloud (CC) and cloud to ground (CG) flashes, the dependence of lightning on the season, location and storm type, etc. In addition to the characteristics of different kinds of flashes, other factors that are associated with flashes like lightning current parameters, electric and electromagnetic fields generated by a lightning stroke or spots with high flash density are also of interest. Investigations about the distribution of the lightning density over a large area, lightning strikes in an elevated terrain or to the wind turbine are also significant for several applications like risk analysis, evaluating the performance of lightning detection systems or climate studies.

Austrian Lightning Detection and Information System (ALDIS) has discovered spots with significant high flash density in Austria. ALDIS noted that tall objects on mountains have a triggering effect to flashes. Flashes to the tower have significantly higher stroke numbers than flashes to the ground in the vicinity of the tower.

In this master thesis, the hypothesis that the electric fields of the first and subsequent strokes of the same channel of a negative CG flash are more similar compared to different channels will be examined. 74 flashes containing 319 strokes in form of binary and video files are provided for the evaluation. These files contain the records of the electric fields and the video of the corresponding strokes. An Excel data sheet containing detailed information about the recorded flashes is provided. This data sheet enables a faster orientation of the flashes and is used as a reference during the analysis of the flashes. For processing and applying statistics to the flashes, scripts in an analysis software called SCILAB are implemented. Subsequently, in order to examine the scripts, the waveforms of each stroke are plotted both, by means of these scripts and by DataViewer. As strokes of some flashes do not coincide with the criteria of the evaluation method, they are discarded and not taken into account in the evaluation. The flashes were evaluated with the help of the chi squares and cross correlation. A comparison between the first stroke versus the first stroke, subsequent versus subsequent strokes of different GSPs of the same flash, the first stroke versus subsequent stroke of the same channel (GPS) and subsequent stroke versus subsequent stroke of the same channel is carried out. Finally, the mean value of the results of the comparisons of these groups are calculated and compared to the hypothesis of this master's thesis.

Acknowledgement

My special thanks go to my supervisor **Dipl.Ing.Dr. Wolfgang Schulz**, who gave me helpful suggestions for problem solutions, discussions and guided me, while I was working on this master's thesis. I wish everyone had a supervisor like him. I also thank **Univ**.**-ProfDr.-Ing Wolfgang Gawlik** because of his concern and help. I would like to thank my wife **Milica Jovanovic** for her patience and unlimited support. My thanks go to my sisters (Syeda Hosneara Chowdhury, Syeda Kaniz Fatema, Nasreen Chowdhury and Syeda Khanom) and all my friends as well as.

Table of Contents

Abbreviations

ALDIS	Austrian Lightning Detection & Information System
CC	Cloud-to-cloud
CG	Cloud-to-Ground
GC	Ground-to-cloud
GSP	Ground striking point
ICC	Initial continuous current
ISS	International Space Station
LF	Low Frequency
LLS	Lightning location system
NASA	National Aeronautics and Space Administration
NRS	No return stroke
TLP	Total Lightning Processor
us, µs	Micro second
VHF	Very High Frequency
VLF	Very Low Frequency

1. Introduction

The existence of lightning and thunder dates back billions of years. Due to its destructive power, lightning became a part of religious belief almost for all ancient civilizations (Rakov and Uman, 2003). In the Middle Ages, the concept of natural catastrophes was not familiar to people, however, there had been wise people like Lucretius in 60 BC who tried to find protection against lightning and many people tried to react against lightning in their own manner (Bouquegneau, 2011). In 1752 Benjamin Franklin designed the first lightning rod after his experiments with a kite. The revolutionary progress in physics, chemistry and technology in the 19th and 20th centuries enabled the investigation of atmospheric physics and lightning more precisely than in the previous time. The streak camera facilitated recording of multiple-stroke flashes; moreover, the USA, Germany, and Russia equipped their power transmission lines with magnetic links. These magnetic links were employed to measure the amplitude of lightning current that strikes power lines (Bouquegneau, 2011).

1.1 Motivation

Because of dangerous nature, lightning and thunder had occupied the mankind since the time before Christ (Bouquegneau, 2011).

According to ÖNORM (ÖVE/ÖNORM 62305-1), there are three kinds of damages caused by lightning, which are:

- injuries of living beings by electric shock
- physical damage to manmade structures
- failure of electric and electronic systems

These damages include the loss of human and animal lives and also an enormous economic loss is counted by crop failure, forest, and house fire. Additionally, lightning causes transient faults and outfall in power transmission grids. The electromagnetic fields which are generated by lightning may have an influence on the operation of electronic systems. According to some studies, there are 24,000 deaths and 240,000 injuries caused by lightning every year worldwide (Holle, 2008). The horizontal extent of a cloud ranges from 10 to 20 km and thus, it is not easy to predict the striking point precisely and also not possible to prevent the whole area from being struck by lightning using a lightning rod. Therefore, the more lightning parameters we understand, more efficiently we can take the precautions against lightning damages.

Up to now, there has been no recognized method to prevent lightning strikes; In order to gain more insight, lightning research institutes all over the world investigate the characteristics of different kinds of flashes, factors that are associated with flashes, like lightning current parameters, electric and electromagnetic fields generated by flashes and spots with the high flash density, etc. The dependence of lightning on the season, location and storm type was analyzed in several papers (Rakov and Uman, 2003). Lightning strikes in an elevated terrain or to wind turbines are of interest for several applications like risk analysis, evaluating the performance of lightning detection systems and climate studies, etc. (Smorgonskiy et al., 2013). ALDIS has discovered spots with significant high flash density in Austria and noted that tall objects on mountains had a triggering effect to flashes (Diendorfer et al., 1997). There is no clear specific evidence on the general geographical dependence of the CG flash parameters, but in some unique cases, lightning exhibits geographical dependence. For instance, lightning in the Alps region shows specific characteristics which are not seen in other regions of the world (Vergeiner et al., 2016).

1.2 Scope and hypothesis

A lightning flash may have more than one stroke. Most of the time a negative cloud to ground lightning flash has usually 3 to 5 strokes. Only less than 20% of the negative cloud to ground lightning exhibit a single stroke (Hanke, 2014). Strokes of a multistroke flash can strike the ground either at the same point or at several points. These points can be separated up to several kilometers. **A flash is considered as an ensemble of all CG strokes that strike within 10 km from each other within a one-second time window** (Cummins et al., 2009).

It is hypothesized that the waveform of the electric field of the first and subsequent strokes of a negative cloud to ground lightning, which use the same channel or GSP, are more similar compared to the waveform of the first and subsequent strokes from different GSPs.

Furthermore, in the same channel, the waveforms of the subsequent strokes are more similar unlike the waveform of the first and subsequent strokes.

Additionally, the waveforms of the first strokes from different GSPs of a flash are less similar in contrast to the waveforms of the first and subsequent from the same GSP. The reason may be that the first strokes with different channels (GSP) have branches, which are visible both, in the sky during the lightning and in the waveform of their electric field. However, the subsequent strokes do not have branches because they use an existing channel. Unlike the first strokes, the waveform of the electric field of the subsequent strokes has fewer spikes, see Figure 5.15.

The focus of this master's thesis lies in the examination of the hypothesis by means of statistics and correlation functions, which will be applied to the field measurement data provided by ALDIS. The measurement of the electric fields of the strokes of each flash was accomplished by means of an electric field measurement system. The provided video files will facilitate verifying if a stroke moves down to the ground using the same channel as the preceding stroke.

1.3 Approach

The provided data contained video records and electric field data of negative CG flashes. Both, video and electric field data are important for the identification of the strokes. The strokes can be identified either on the video or in electric field data and sometimes they are present in both data set (Schulz et al., 2012). Each file is ordered by occurrence time, date, and contains a record over a time interval of one second and may contain several strokes. We will examine the electric fields and the videos of each flash by means of software tools. As each file contains data for a time interval of one second, it may be possible that possible that some flashes are stored in two or even in three consecutive files. Whenever the electric fields of the strokes of a flash are stored in two or three consecutive files, it is tedious to make a visual comparison of all electric fields together. On one hand, the waveforms of the electric fields are separated by their occurrence time. On the other hand, they will be plotted in several graphics' windows. A better visual distinction can be made when the electric fields are aligned in the same way and plotted over each other in the same graphics window. This problem will be remedied with the help of software and some implemented scripts that allow clipping and saving these electric fields separately, and additionally, plotting the electric fields both, together or individually. A visual and numerical (quantitative) similarity check of the electric fields of the strokes will be run by means of some mathematical and statistical functions, which will be discussed in the subsequent chapters.

1.4 Outline

Chapter 2 provides a basic overview of terminologies. This chapter also presents basic information about physics of thunderclouds and lightning, afterwards, describes the type of lightning discharge.

The aim of Chapter 3 is to introduce the available lightning detection systems, their operation principle. Additionally, this chapter also gives a brief description of international and Austrian lightning location network.

Chapter 4 describes analysis methods, which are used for the data processing and evaluation, subsequently justifies the selection of the method which will be used to work out this master's thesis.

Chapter 5 deals with the analyses and processing of the flashes using the video files and the electric field data. Besides the introduction of the implemented functions, also the processing of the strokes for the evaluation using the implemented functions is described here.

Chapter 6 presents the results of the chi squares and the cross correlation and the mean value of these results. Subsequently, the mean values are validated against the hypothesis of this master's thesis.

Chapter 7 gives the conclusion of this work and subsequently discusses the limitations which have been encountered during the elaboration of this master's thesis. Ideas and improvement proposals for future work will also be discussed.

2. Physics of thunderclouds and lightning

This chapter provides basic knowledge about lightning physics and the physics of thunderclouds. Section 2.1 explains several terminologies and definitions which are very often used in the field of lightning research and which are also relevant for the thesis at hand. Section 2.2 focuses on lightning physics. In Sections 2.3 to 2.5, the following topics “Formation and type of thunderclouds”, “Negative and positive downward lightning discharge” and “Human initiated lightning discharged” will be treated.

2.1 Terminology

The following definitions below are also available in (Rakov and Uman, 2003), (Graham et al., 1997) and (Hanke, 2014).

Flash: an entire lightning process, regardless if it touches the ground or not.

Stroke: refers to the components of a cloud to ground discharge.

First stroke: comes out with a stepped leader. This is an optical intermittent process; because of this, it is called a stepped leader.

Return stroke: a stroke consists of a downward stepped leader and an upward return stroke.

Continuing current: is a relatively low-level current which may be generated immediately after the return stroke.

M-component: when a lightning channel carries continuing current, transient processes take place within the channel. These transient processes are called M-components.

Subsequent stroke: a stepped leader initiates the first stroke and moves down to the ground, whereas the subsequent strokes are initiated by a dart or dart stepped leader in an already existing channel.

2.2 Type of lightning discharge

There are four types of lightning discharges between a cloud and the earth which are classified based on the polarity of the charge effectively lowered to the ground and the propagation direction of the initial leader. They are called as follows:

- downward negative lightning
- upward negative lightning
- downward positive lightning
- upward positive lightning

These four types of lightning are depicted in Figure 2.1. Figure (a) represents downward negative lightning; 90% of global CG lightning are downward negative lightning discharge. The other 10% belong to downward positive lightning which is illustrated by type in Figure 2.1(c). For upward positive or negative lightning, elevated objects (higher than 100 m) or objects of moderate height on mountain tops are necessary. Types (b) and (d) correspond to these flash types.

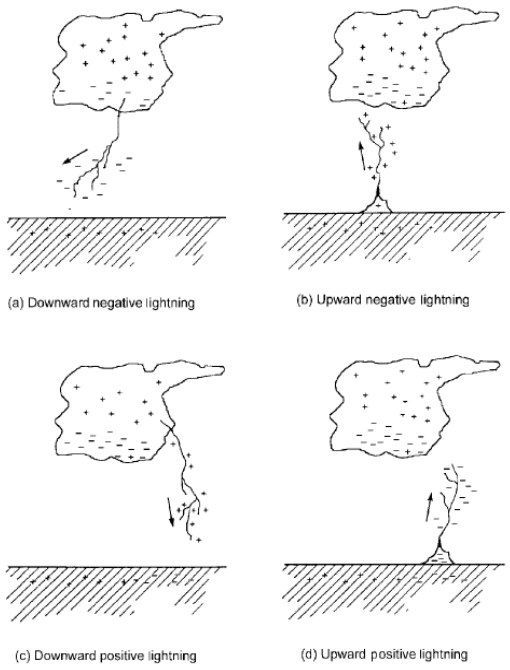

Figure 2.1: Four types of cloud- to-ground lightning showing the direction of the initial leader and the cloud charge lowered to the ground. Adapted from (Rakov, 2003)

The bipolar lightning discharge involves both, positive and negative charges. Intercloud, intracloud and cloud-to-air discharges do not strike the ground.

2.3 Formation of thunder clouds and lightning current

The generated current in a lightning channel is a result of lightning discharge and it is a function of height and time. The peak current determines the maximum voltage drop across an earthing resistance. The charge influences the melting process at the attachment point of the lightning channel. The maximum steepness of lightning current determines the maximum voltage magnetically induced into open loops.

A thundercloud referred to as lightning producing cumulonimbus can only be formed while the atmosphere is unstable. This occurs, when the atmospheric temperature lapse rate is higher than the moist adiabatic lapse rate or saturated adiabatic lapse rate of about 0.6 °C per 100 m. In that case, parcels of moist air can rise and cool by adiabatic expansion. The condensation on airborne particle takes place and the visible cloud begins to form (cumulus. Above 0 °C isotherm not all particles freeze, some remain liquid in form of cooled water particles. Below -40 °C all water particles are frozen. The range between 0° and -40 °C is responsible for most of the electrification processes within the thundercloud. Figure 2.4.b shows the charge distribution in a thundercloud.

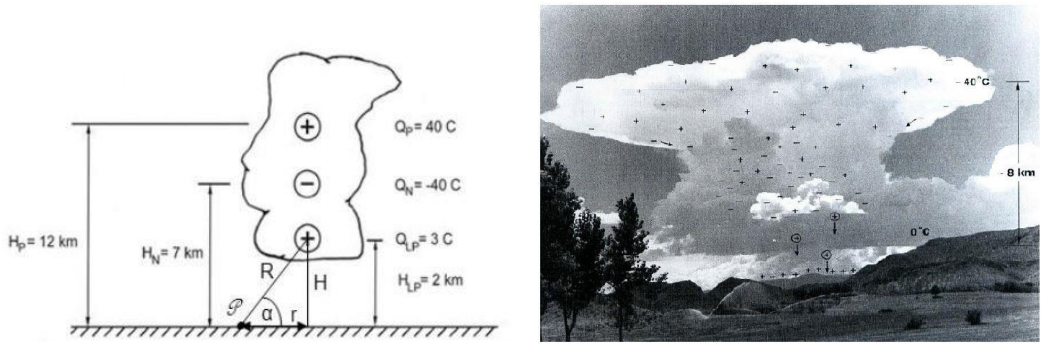

25.a **24.b**

Figure 2.2: a. Vertical tripole adapted from (Rakov and Uman, 2003**), b.** Charge distribution in a thundercloud adapted from (Krehbiel, 1986)

The coarse charge distribution in a thundercloud can be assumed as tripole which is illustrated Figure 2.4.a. There are two main charged regions, a positive on the top and a negative in the middle, where the temperature ranges between -10 and -25 °C.

The graupel-ice mechanism is believed to be the main charging mechanism. In this mechanism large precipitation particles (hydrometeors with fall speed ≥ 0.3 m s^{-1} (Rakov and Uman, 2003)) collide with small ice crystals in the presence of water droplets, which are important for the charge transfer. The lower positive charge probably originates also from upward carried corona charges from the ground and positive ions which are generated by cosmic rays. The second mechanism is called convection mechanism, takes place when positive fair-weather charges are carried to the top of the forming

cumulus. Those charges attract negative charges produced by cosmic ray to the cloud's boundary. Downdrafts carry the negative charges down the sides of the cloud to the base.

A negative downward lightning flash is assumed to be initiated by an initial break down or preliminary breakdown. It is presumed by some researchers that the electric fields are enhanced by the emission of the positive corona from the surface of precipitation particles. Runaway electrons released also contribute to the initial breakdown. Presumably, a sequence of channels spread from the cloud charge source from the preliminary breakdown, and one of those channels develops into the subsequent downward stepped leader. In Figure 2.6, the preliminary break down, attachment process, return strokes, K- and J- etc. are illustrated.

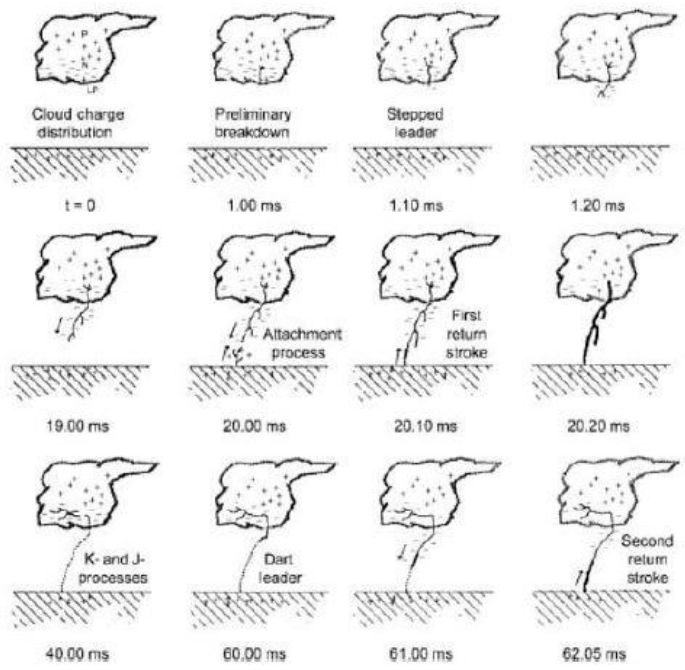

Figure 2.3: Various processes taking place during a negative cloud to ground lightning adapted from (Rakov and Uman, 2003)

The stepped leader propagates toward the ground in a series of steps with step lengths in the range of tens of meters and a step duration of typically about 1 μs. Physically, a stepped leader is composed of a negatively charged plasma channel. There are two categories of leader: α and β-Type (Hanke, 2014). A positive upward leader is launched from the ground and initiates the attachment process with the downward stepped leader. After the attachment process, the return stroke takes place transporting the negative charges stored on the channel to ground. Not always are all negative charges neutralized. The speed of the return stroke is in order of between one third and one half of the speed of the light. The maximum current flows through the channel while the first return strokes are heating the channel up to 30,000 K and create a channel pressure of 10 atm (~ 1MPa). This channel pressure causes a shock wave which is known as thunder. The J-Process is initiated during the end of the return stroke and the beginning of the following dart leader, see Figure 2.6. During the J-Process (J is for Junction), the

charge in the cloud is redistributed and no luminous channel between cloud and ground is formed. A return stoke is often followed by a continuing current which typically lasts for tens to some hundreds of milliseconds with currents in the range of 100 to 200 A. Continuing currents flow through an already existing path and causes severe damages (Hanke, 2014).

2.4 Positive and bipolar downward lightning discharges

Positive charges are transported from the cloud to ground by a positive flash can cause more severe damages than negative lightning. Because the current which flows during a positive lightning can range up to 300 kA. During the cold season, positive lightning is the dominant type of CG discharges, and has an upward connecting negative leaders that are up to 2 km long.

Bipolar lightning discharge to the ground is characterized by a polarity reversal in the lighting current during a discharge. Bipolar lightning is commonly observed in upward-initiated lightning. The current profile of a bipolar and an upward negative flash is demonstrated in Figure 2.7.

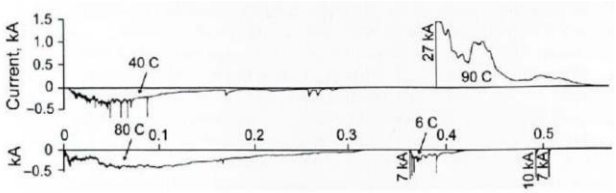

Figure 2.4: Picture top depicts the current profile of a bipolar upward flash. The waveform below visualizes the current of a negative upward flash. The time-scale is in second. Adapted from (Rakov and Uman, 2003)

2.5 Upward-initiated lightning discharges

Upward negative lightning involves elevated objects with heights less than 100 m like towers, etc. Upward lightning also occurs in rocket triggered flashes. An upward positive leader initiates an upward negative lightning which transports a negative charge to the ground. The same process happens in case of an upward positive lightning, except the polarity is reversed. An upward leader serves to form a conducting channel between the cloud charge region and the grounded object. Through this channel the initial continuous current flows for some hundreds of milliseconds e.g. 10 to 1 kA.

3. Lightning detection systems

This chapter deals with the devices employed for lightning detection. Section 3.1 describes the lightning location techniques. The overview of some LLSs is given in subsection 3.2. Subsection 3.3 gives a brief description of the international lightning detection networks and of ALDIS.

3.1 Lightning location techniques

Lightning flashes radiate electromagnetic energy over a wide range of frequencies. Due to this, different types of sensors and networks need to be applied for different frequency ranges (Cummins et al., 2009). An overview of different lightning locating techniques and the lightning power spectrum is given in Figure 3.1. Preliminary, breakdown processes and stepped leaders of a negative CG flash at their beginning emit radiation in VHF band. Dart leaders, recoil streamers and stepped leaders show continuous radiation bursts while they are approaching the striking location.

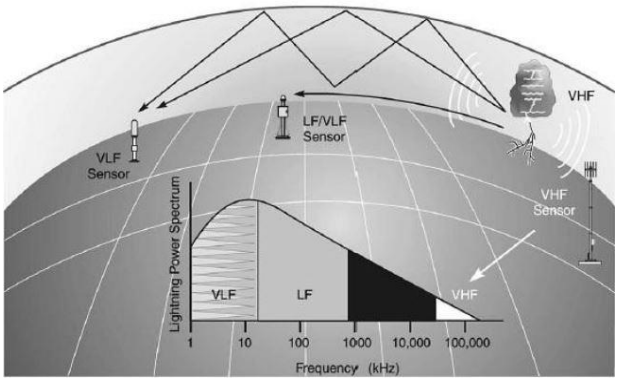

Figure 3.1: Operation frequencies of LLS. Adapted from (Cummins et al., 2009)

High current components of the lightning discharge exhibit very little VHF activity. However, they emit radiation in VLF/LF range. It is visible in Figure 3.1 that VHF sensors are limited by line-of-sight propagation. Thus, they are sensitive to leaders and breakdown processes. On the other hand, vertically polarized transient pulses in the VLF/LF ranges propagate along the surface of the Earth,

which requires that no elevated objects block the propagation. Sensors of these ranges are appropriate to detect return strokes in CG flashes. Along the surface of the Earth, VLF signals also propagate by reflection between the ionosphere and the ground. Because of this, they can still be detected at a great distance from the striking point.

Magnetic direction finding (MDF) is operated on the basis of the magnetic direction finding receivers. Two vertical and orthogonal loops, one orientated North-South and the other East-West measure magnetic fields from a lightning discharge.

Time of arrival technique (TOA) has two type, one functions at VHF and the other at VLF/LF range. TOA is based on the measurement of runtime differences.

Interferometry is used to detect noise produced by dart leaders and measures the phase difference between narrowband signals using a phase detector, which compares the output signal of the antennas.

Electric and magnetic field amplitude techniques determine the location of a lightning discharge by measuring the electric or magnetic field amplitude.

Ground-based optical direction finding uses optical signals to determine the direction to a lightning discharge. Specific photographic cameras, television cameras and photoelectric detectors are used.

Space-based lightning detection is achieved with the help of satellites.

Stand-alone-lightning-detection these are detectors, which are capable to detect both, direction and distance (Hanke, 2014).

3.2 Overview of some Lightning Location Systems

More than 60 LLS networks worldwide are equipped with the lightning detection sensors operating in the VLF/LF range. In Europe, 19 national lightning detection networks collaborate within the EUCLID (European Cooperation for Lightning detection) network. Other large lightning location networks are e.g. JLDN (Japan Lightning Detection Network), NALDN (North American Lightning Detection Network), etc. The performance analysis of the EUCLID network published in March 2016, demonstrates a significant improvement over the last seven years (Schulz et al., 2016).

3.3 The lightning location network of ALDIS

ALDIS was founded 1989 under the initiation of Dr. G. Diendorfer. The ALDIS network is one of the networks with the shortest sensor baselines (in the range of about 120 km) and therefore one of the highest resolution networks in the world (Cummins et al., 2009). Figure 3.2 shows the ALDIS sensors locations in Austria.

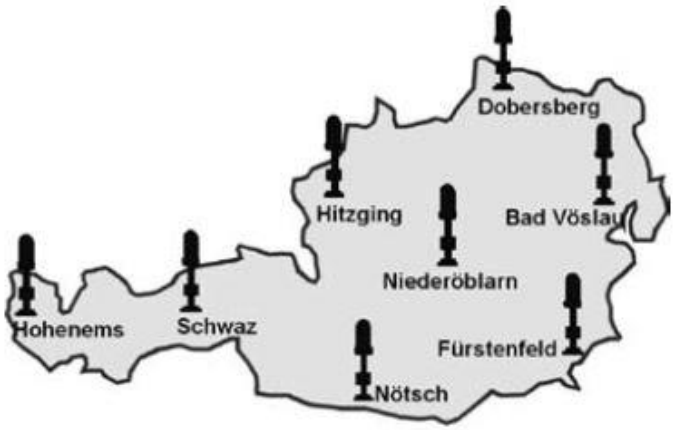

Figure 3.2: The locations of ALDIS lightning sensors. Adapted from (Diendorfer and Schulz, 2008)

4. Analysis methods

Software was needed for playing the video files and visualizing the waveforms of the electric fields of the strokes. Usual software tools as e.g. MiDas Player 2.1.7 (for playing the video) [16] and DataViewer 1.4 (for plotting the waveform of the electric fields) were used by ALDIS [2], [17]. Section 4.1 gives an overview of some common statistical distribution functions. Section 4.2 outlines the argumentation about the analysis method used in this master's thesis. Furthermore, a brief description of the application of the correlation function is also given in this section.

4.1 Statistical distribution function

Before we start analyzing the data using a statistical distribution function to which the data can be fitted [13], we must first consider the following issues below:

- Do the data have discrete or continuous values?
- The Symmetry of the data
- How frequently have the data extreme values.

The data for the investigation were captured with a sample rate of 5MS/s. The upper and lower frequency limit of data is constrained by the integrator of the recording system. The electric fields of the strokes have continuous values and no symmetry. There are a lot of statistic distribution functions. In the following chapters, the characteristics of some common statistic distribution functions will be discussed.

4.1.1 Binomial distribution

A **binomial distribution** consists of 'n' identical trials. Each trial results in one of the two outcomes, called failure and success. The probability of success remains the same from trial to trial. Each trial is independent, and the outcome of any trial does not affect the outcome of others [8]. The probability

of getting exactly ‘k’ successes in ‘n’ trials can be counted using this binomial distribution below [George et al. 1960].

$$P(k,n,p) = \binom{n}{k}.p^k.(1-p)^{n-k} \quad 4.1$$

$\binom{n}{k} = \frac{n!}{k!(n-k)}$ Is the binomial coefficient

The formula describes the following: ‘k’ successes occur with the probability p^k and (n-k) failures occur with the probability $(1-p)^{n-k}$ whereas k=0, 1, 2, 3, … integer number. ‘k’ successes can occur anywhere within ‘n’ trials.

4.1.2 Poisson distribution

The **Poisson distribution** is a discrete probability distribution that expresses the probability of a given number of events occurring in a fixed interval of time, if these events occur with a known constant rate. The Poisson distribution is used where the frequency of events is viewed over a certain period of time and mostly is invoked for rare events. The required key parameter is the average number of events in the given interval λ. For the Poisson distribution, the events must be a whole number, occurrences are independent and the average frequency of the occurrence for the time period in question is given (Haight, 67), [9]. The equation 4.2 depicts the formula of the Poisson distribution. $\mathbb{N}_0$ represents all natural whole numbers including zero.

$$P(\mathrm{X} = x) = \frac{\lambda^x}{x!}.e^{-\lambda}\,,\ x \in \mathbb{N}_0 \quad 4.2$$

λ is the average number of events per interval

x is the number of times an event occurs in an interval

4.1.3 Hypergeometric distribution

The **Hypergeometric distribution** measures the probability of k successes in ‘n’ draws without replacement from a finite population of size N that contains exactly K successes, whereas each draw is either success or failure [10]. The formula of the Hypergeometric distribution function is given below.

$$P(X = k) = \frac{\binom{\mathrm{K}}{\mathrm{k}}*\binom{\mathrm{N-K}}{\mathrm{n-k}}}{\binom{\mathrm{N}}{\mathrm{n}}} \quad 4.3$$

N is population

n is number of draws

K is number of success in population N

k is number of success came in draws

4.1.4 Normal distribution

Among the statistical distribution functions, the **normal distribution** is the most commonly used distribution function, also known as the **Gaussian distribution**. This probability distribution function is symmetric, it plots all of its values in a symmetrical fashion and most of the results are situated around the probability's mean. It is bell shaped, and continuous for all values of X between $-\infty$ and ∞. Two parameters μ (mean value) and σ (Standard deviation), determine the shape of the distribution curve. In the Gaussian distribution, the mean value is equal to zero, while the standard deviation is equal to one [11], [12], [13]. The formula below represents the normal distribution function.

$$f(x;\mu,\sigma^2\ ) = \frac{1}{\sqrt{2\pi\sigma}}.e^{-\frac{(x-\mu)^2}{2\sigma^2}} \qquad 4.4$$

4.1.5 Chi Square distribution

Depending on the context, the chi square distribution is applicable for a large and small number of samples. There are a few variations on the chi square distribution; depending on the collected data and the hypothesis to be tested can a particular variation be used. The basic concept of all variations is comparing the observed value to the expected value [5].

- A chi square distribution for goodness of fit is used to decide whether there is any difference between the observed value and the expected value.
- A chi square distribution for independence compares two variables in a contingency table to see if they are related. This is a nonparametric test.
- The chi square distribution for Homogeneity answers the proposition that the several populations are homogeneous with respect to some characteristic.
- The chi square distribution for single variance is used to test a hypothesis on a specific value of the population variance.

The data to be used must be random, raw, mutually exclusive, taken from independent variables and drawn from a large enough sample. **A small value of a chi square means that the observed data fits to the expected data and indicates a relationship between them**. **Unlike a small value**, **a large**

value means that there is no existence of a high correlation between the data. The formula below depicts the chi square distribution.

$$X^2 = \sum_{i=1}^{N} \frac{(O_i - E_i)^2}{N} \quad 4.5$$

The subscript 'i' is the data item number. 'O' and 'E' and 'N' are respectively the observed, expected values and total sample number. The summation symbol indicates that a calculation for every single data item of the data set must be performed.

4.2 Analysis methods used in this thesis

This section presents the analysis methods, which will be deployed for the evaluation of the data.

4.2.1 Comparing data by calculating chi squares

In order to prove the hypothesis of this master's thesis the following will be compared:

- the waveforms of the electric field between the first and subsequent stroke in the same channel
- the waveforms of subsequent strokes of the same channel
- the waveforms of the first strokes with different GSPs of each flash
- the waveforms of subsequent strokes with different GSPs of each flash

The binomial distribution and the hypergeometric distribution do not perform this kind comparison. The probability or counter-probability for the success or failure of the trial and the number of trials must be given, so that the number of successes or failures can be counted. The use of the Poisson distribution will not be an appropriate solution. Additionally, it does not allow distinguishing between two variables with large samples. Applying the Normal distribution will not be a means to achieve the goal as well because it also does not enable comparing two variables with large sample.

As each waveform consists of several samples, e.g. 4000 samples, due to this, each sample of these waveforms needs to be compared. Thus, the comparison, using the chi square fits best. The similarity of the waveforms of the strokes will be compared by determining the chi squares, that is a number relates to the similarity of the comparing waveforms. However, to get an overall conclusion about different groups of strokes, e.g. first stroke versus subsequent strokes of the same channel, the mean chi squares for each of those groups must be calculated.

4.2.2 Comparing waveforms by cross correlation

Apart from the numerical evaluation of the similarity of the strokes, it also needs to be analyzed graphically and quantitatively, how similar the waveforms are to each other. With the help of the cross correlation function, it can be found in which lag of the time axis the waveforms of two strokes are more similar. A positive correlation coefficient indicates a positive relationship between the variables. A negative coefficient, on the contrary, means a negative relationship [14]. There is a perfect degree of association when the value of the correlation lies around ±1, whereas there is a weak relationship when the value goes toward zero. A sharp peak of the correlation curve above zero of the horizontal axis means two waveforms are very similar and they have no phase shifting. The width of the curve shows how long the two signals remain the same when these signals are moving against each other (Papula, 2001), (Weyerhäuser, 2005), (Mazzoni, 2010). The correlation between signals with different lengths can be performed under the condition that the signals have the same sampling rate [4]. Due to no difference between the involved signals, autocorrelation yields always the maximum value one. The equation 4.7 depicts the formula of the normalized cross correlation. X and y are two random variables, in case of the autocorrelation x=y.

$$r(\tau) = \frac{\int_0^T x(t)y(t+\tau)dt}{\sqrt{\int_0^T x(t)*x(t)dt} * \sqrt{\int_0^T y(t)*y(t)dt}} \qquad 4.7$$

In Figure 4.1, the autocorrelation of the stroke N97F1 and the cross correlation between the strokes N97F1 and N97S1b are respectively illustrated in black and violet. The maximum value of the black curve, which represents the autocorrelation of the stroke N97F1, is one. Each half of the horizontal axis of the diagram is divided into the total number of the samples comprised by the time duration. The wide area under the black curve indicates that a big part of the waveforms is similar which is yielded by the correlation of the stroke N97F1 with itself. Unlike the black curve, the violet curve, which represents the cross correlation showing an unsymmetrical shape, has got a lower value of about 0.68 and a smaller area under the curve than the black one, because the waveforms of the strokes N97F1 and N97S1b are quite different, see the red and green curve in Figure 5.17.

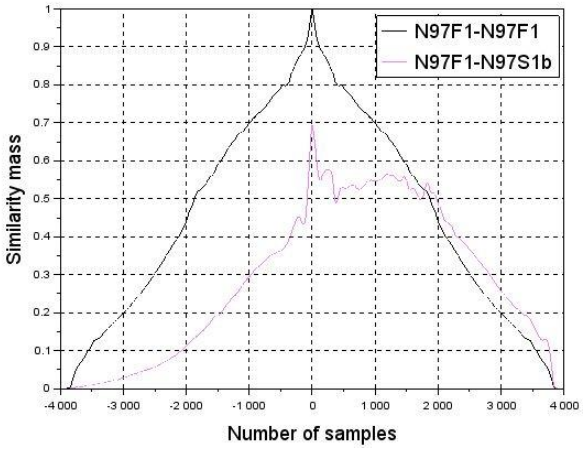

Figure 4.1: Autocorrelation of stroke N97F1 and cross correlation between strokes N97F1and N97S1b

5. Flash analyses and processing

Before the applying statistics to the data, the strokes of the flashes will be organized and prepared, which will ensure a clear overview and a shorter computation time. Section 5.1 gives general information about the provided data. Section 5.2 analyzes the video records of the corresponding flashes. For this, the software tools: MiDas Player and DataViewer will be used. Section 5.3 outlines the scripts implemented in SCILAB which will be deployed for the data processing and evaluation. Section 5.4 introduces the processing of the electric field data of the strokes for the evaluation. Besides normalizing and fixing the alignment of the peak of the electric fields, also the offset compensation and the criteria for the discarding of strokes are described here. Section 5.5 deals with data selected for the evaluation.

5.1 General information

The flashes were recorded in Austria by means of a mobile video and field recording system positioned in rural areas in the year 2010 and 2012 during the months of June and July. An excel data sheet containing detailed information on the recorded flashes was provided. This information provided a basis to analyze the flashes using the video and the electric field data files. Besides the flash number, both, the electric field and video file names show an additional sequence number. Some important information about the flashes included in the data sheet are:

- flash number
- occurrence date and time of flashes
- striking time of strokes in nanoseconds
- longitude of the striking point
- latitude of the striking point
- peak current (including its sign)
- multiplicity
- number of strokes within a flash
- stroke per striking point

- distance between the lightning detection sensor of the mobile station and the striking point of the strokes
- order of the strokes of each flash
- flash classification inter cloud (IC) or cloud to ground (CG).

Flashes detected within the distance between 15 and 65 km were considered for the evaluation. As a result, 74 negative CG flashes containing 319 strokes out of the provided data were selected for the analysis. Among 74 flashes, 38 were detected in the year 2010 and the rest in 2012. Flashes from the year 2010 were registered in the following places: Kulm bei Weiz, Obervellach/Mölltal, Murau, Kalsdorf/Graz, Arzberg and Hammersberg, whereas the flashes from the year 2012 were detected in Altenbach, Loosdorf and Wr. Neustadt. 319 strokes of the 74 flashes are broken down by the detection year and the range at which these flashes were detected. Figure 5.1 displays the number of the strokes ordered by the detection year and the detection range.

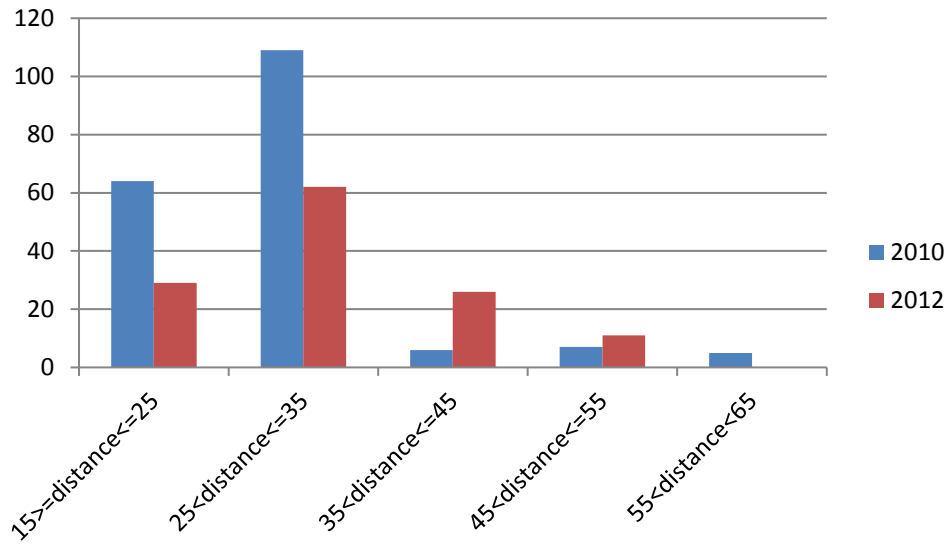

Figure 5.1: The strokes of 74 flashes distributed by the detection year and distance in [km]

The flashes are classified in terms of the number of their first and subsequent strokes and listed in Table 5.1

Table 5.1: List of the flashes with their first and subsequent strokes

Number of flashes	Single GSP	Multiple GSPs	Multiple subsequent stroke at same GSP	Multiple subsequent strokes at multiple GSPs	Single subsequent strokes at same GSP
19	-	✓	-	-	-

7	✓	-	-	-	✓
12	-	✓	-	-	✓
16	-	✓	✓	-	-
15	✓	-	✓	-	-
5	-	✓	-	✓	-

As Table 5.1 shows, there are 19 flashes, each of them has multiple GSP, however no subsequent stroke. Seven flashes, each of them has one GSP containing a subsequent stroke. Twelve flashes, each of these flashes has multiple GSPs but one subsequent stroke. Twelve flashes, each of these flashes has multiple GSPs and every GSP has one subsequent stroke. There are sixteen flashes, each of them exhibits one GSP with multiple subsequent strokes. Fifteen flashes, each of which has a single GSP with multiple subsequent strokes. Each of the remaining five flashes in the last line of the table contains multiple GSPs and subsequent strokes at multiple GSPs.

5.2 Flash analysis based on video and electric field data

The electric field data together with the video recordings allow a straightforward correlation of each individual stroke detected by the LLS (Schulz et al., 2012). A stroke in the graphics window of the DataViewer can be found at the time which corresponds to the striking time in the column "Nano" of the excel data sheet, see figure 5.2. Figure 5.2 depicts an extract of the excel data sheet. The flashes N97 and N98 and the columns with the important flash parameters are visible in this figure.

LLS Data

Data Nb.	Date	Time	Nano	Longitude	Latitude	Peak Current	Distance	Num	ns	sn	calcul	nbdf	m	Single stroke Flash	Completely correct detected stroke	Peak Current detected strokes	Comment	Ground strike points	LDA	Strokes per Strikept	Comment
N97	18.06.2010	150148	540590741	15,9761	47,633	3,4	48,4	124811	1	1	114	2					Auf Kamera und Feld nichts zu erkennen				
	18.06.2010	150149	138889695	15,5909	47,4193	-25,6	24,5	124824	3	1	114	19	3		1	-25,6	eindeutig Entladung zu erkennen, Kamera und Feld	1	F1	3	deutlich sichtbar
	18.06.2010	150149	416725991	15,5981	47,4213	-5,4	24,4	124824	3	2	114	5			1	-5,4	eindeutig Entladung zu erkennen, Kamera und Feld		SUa1		deutlich sichtbar
	18.06.2010	150149	450964541	15,5857	47,4202	-9,8	24,8	124824	3	3	114	10			1	-9,8	eindeutig Entladung zu erkennen, Kamera und Feld		SU1b		deutlich sichtbar
	18.06.2010	150149	139266355	15,669	47,265	3,8	7,3	124825	1	1	78	2									
N98	18.06.2010	150251	991107110	15,5084	47,404	-14,0	26,8	125131	2	1	114	11	2		1	-14,0	eindeutig Entladung zu erkennen, Kamera und Feld	2	F1	1	deutlich sichtbar
	18.06.2010	150252	340588398	15,5968	47,418	-9,9	24,2	125131	2	2	114	8			1	-9,9	eindeutig Entladung zu erkennen, Kamera und Feld		F2	1	deutlich sichtbar

Figure 5.2: Extract of the excel data sheet with the flashes N97 and N98

The procedure of the flash analysis with respect to the videos and electric field will be described using the example of the flash N97, which was detected by ALDIS in Austria on 18.06.2010, at a distance of 24.4 km from the location Kulm bei Weiz. All three strokes (F1, SU1a and SU1b) of N97 struck at

15:01:49 UTC. In order to save the space on the excel data sheet, the time is written without colon, just like 150149. Figures 5.3 and 5.4 respectively show the selection of the files with the video record and the electric field data using the graphical user interface of the MiDAS Player and the DataViewer.

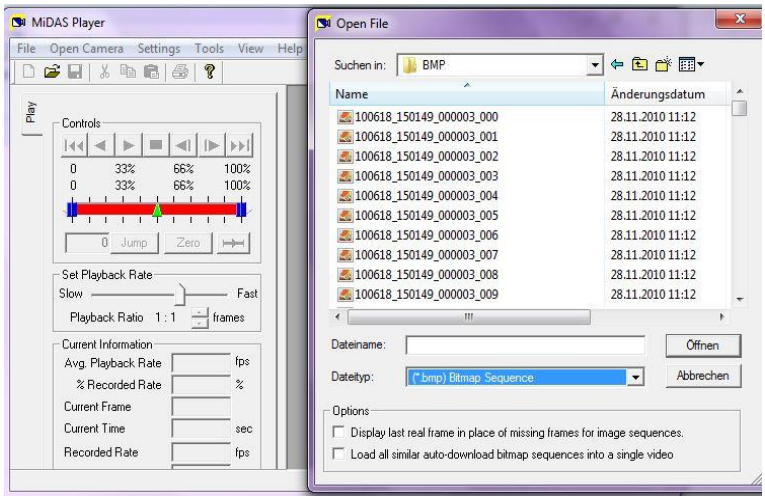

Figure 5.3: Opening video file of the flash N97 using MiDAS Player

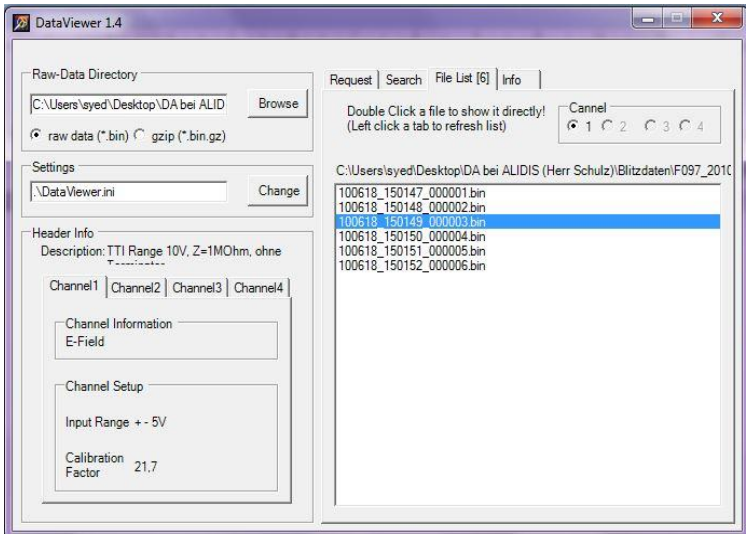

Figure 5.4: Loading binary files with electric field data of the flash N97

Figure 5.5 shows the strokes of the flash N97 in the graphics window of the DataViewer. The time axis of the DataViewer graphics window exhibits a microsecond time resolution. The cursor (in yellow color) is positioned on the electric field of the first stroke. As can be seen in the figure, all strokes of the flash N97 took place within the same second. Due to a compact time resolution, the waveforms of the strokes are not apparent in the figure. However, the vertical green lines indicating the negative

peak values are visible in this figure. Because of atmospheric electric sign convention, the electric fields of the strokes have the negative sign. In Figure 5.6, the video images and the respective electric fields of the strokes F1, SU1a, SU1b are illustrated. Each electric field is zoomed and clipped from the window of the DataViewer.

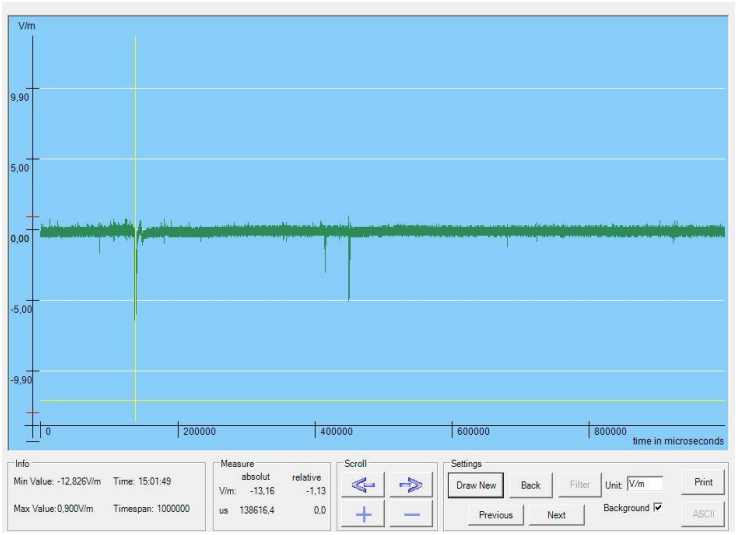

Figure 5.5: Electric fields of the flash N97 in the graphics window of the DataViewer

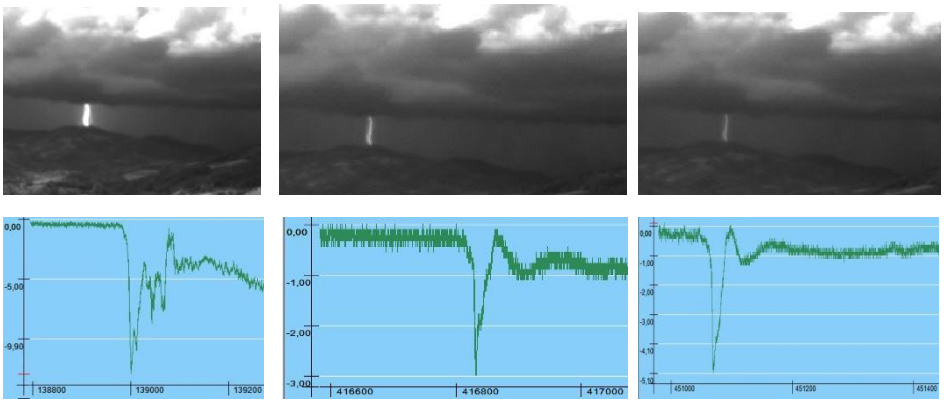

1st stroke F1 **2nd stroke SU1a** **3rd stroke SU1b**

Figure 5.6: Video images and correlated electric field data for the flash N97 (18.06.2010 15:01:49 UTC)

After the examination of the 74 flashes, it can be stated that all strokes could be recognized in their respective video and electric field data files. With this examination, the consistency between the excel data sheet and the electric field data could be verified. Moreover, all the electric fields displayed by

DataViewer can be used as a reference to verify the waveforms plotted by our implemented functions later.

5.3 Implemented SCILAB scripts

This section describes the scripts implemented in SCILAB for preparing the data. The functions and the services provided by these scripts are:

- **flashEvaluation** is the main script. The functions and the services of the other scripts can be obtained by means of this script.
- **plotEFieldOfFlashFromBinaryFiles** reads the electric fields of the strokes from the binary files and save these fields as SCILAB variables.
- **plotEFieldOfFlash** plots the electric fields and the correlation diagram of each stroke of a flash individually for the given time length.
- **applyStatisticToData** is responsible for analyzing the data with the help of statistical functions.
- **closeGraphicWindow** closes all opened graphics windows.

For the execution of the script flashEvaluation, it is necessary to change to the directory with the implemented scripts. All scripts, including the flashEvaluation will be executed by typing the following command exec('C:\Users\syed\Desktop\flashEvaluation',-1) in the command line of the console. Afterwards, a menu with instructions for the selection of the menu options will appear on the console. Figure 5.7 visualizes the execution of the script flashEvaluation on the console, while Figure 5.8 shows the menu appears on the console after the script has been executed.

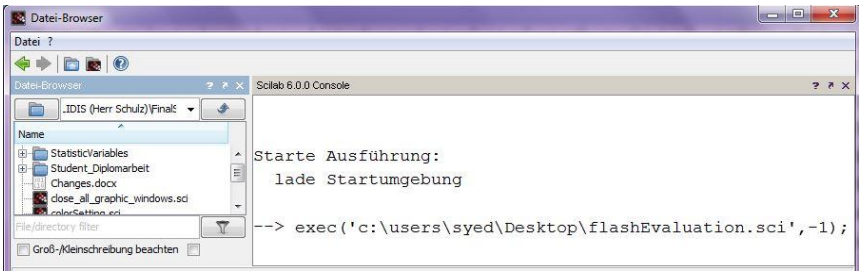

Figure 5.7: Executing the script flashEvaluation from the command line of the SCILAB console

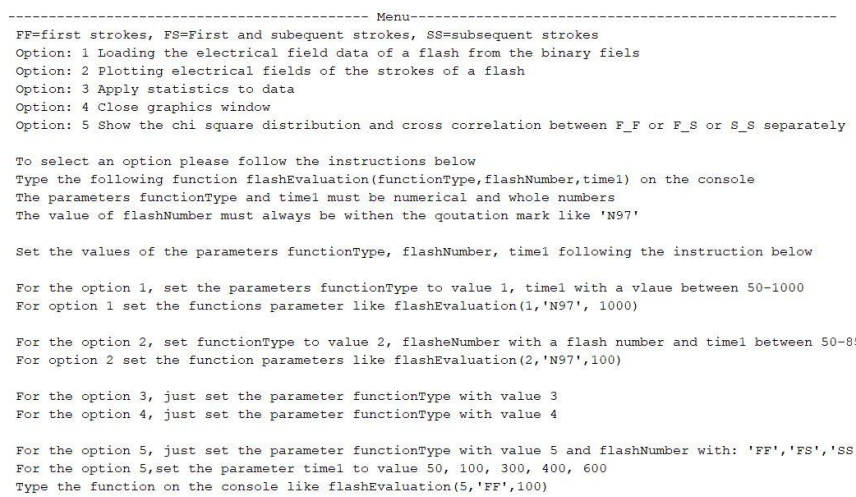

Figure 5.8: Menu with instructions appears after executing the script flashEvaluation

Options which can be selected from the menu are:

1. Loading electric field data of a flash from the binary files
2. Plotting the electric fields of the strokes of a flash
3. Apply statistics to data
4. Close graphics window
5. Show the chi squares and cross correlation between the first versus first, first versus subsequent and subsequent versus subsequent strokes.

The selection of the menu option in Figure 5.8 is described below:

- Option one from the menu will be selected by setting the first parameter “functionType” from the left in the function bar of the flashEvaluation(functionType, flashNumber, time1) to value 1, the middle parameter “flashNumber” with a flash number e.g. “N97” and the last parameter “time1” to a value between 50 -1000.
- Option two will be selected by setting the first parameter to value 2, the middle parameter “flashNumber” with a flash number and the last parameter to a value between 50 -850.
- Option three can be selected, if the first parameter will be set to value 3. For option three the middle and last parameters can have any value because they will be neglected.
- Option four requires the parameter “functionType” to be set to value 4, while the other parameters can remain with their previous values.
- Option five will be selected by setting the first parameter to value 5, the second parameter to value ‘FF' or ‘FS' or ‘SS' and the third parameter to one of these values: 50, 100, 300, 400, 600.

Figures 5.9 a, b, c, and d visualize selecting the menu options by setting the correct parameter value on the console.

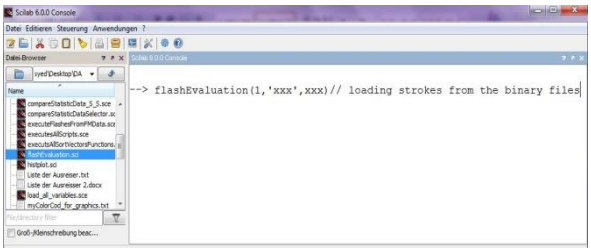

a. Selecting option one

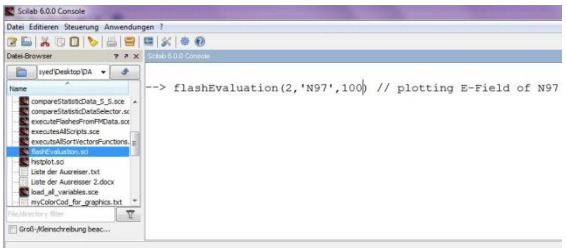

b. Selecting option two

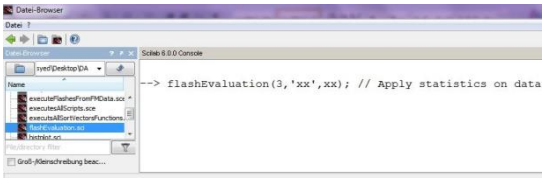

c. Selecting option three

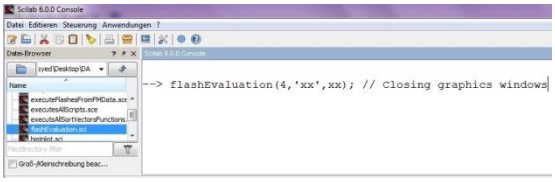

d. Selecting option four

Figure 5.9: Selecting menu options using the function flashEvaluation on the console

A brief description of the other scripts is given below.

The script **loadEFieldFromBinaryFile(**flashNumber, time1**)** is responsible for reading the electric field data from the binary files and saving them as SCILAB variables with the corresponding flash number and stroke order. The flash and the time length of electric field will be selected according to the values of the function parameters "flashNumber" and "time1". In case of the strokes of a flash, which are saved in two or three consecutive binary files, they are copied from the binary files separately, then saved together in one file. This concept increases the simplicity, improves the overview of the strokes and shortens the processing time.

In Figure 5.10, the script loadEFieldFromBinaryFile(flashNumber, time1) and its sub functions readFiles(), clipStrokes(fNr, time1), and saveStrokes() can be seen. The sub function readFiles() reads the strokes from the binary files, while the sub function clipStrokes(fNr, time1) selects and clips the strokes regarding the value of the function parameters fNr and time. The sub function saveStrokes() saves these clipped strokes. A report is displayed on the console, whenever all the strokes of the flash are processed, see Figure 5.11.

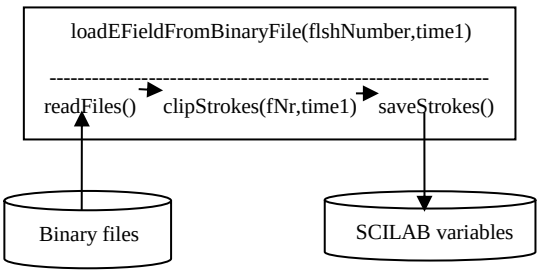

Figure 5.10: Loading files with the electric field data of strokes and saving them as SCILAB variable

```
--> flashEvaluation(1,'xxx',1000)

Measurement_Header = TTI Range 10V, Z=1MOhm, ohne Terminator
Ch1_Header         = E-Field
Ch1_Range          = 10000
Ch1_CalFactor      = 0.021700
Ch1_Datum          = 20100618
Ch1_Time           = 150251
Ch1_Time           = 150252

The strokes N98F1 and N98F2 are clipped for the time sapn of:1000 us

Name                    Type           Size            Bytes
-------------------------------------------------------------
N98F1                   double         1 by 5001       40008
N98F2                   double         1 by 5001       40008
```

Figure 5.11. The report after processing the strokes of the flash N98 is output on the console

The script **plotEFieldOfFlash(**flashNumber, time1**)** loads the strokes of each flash, which have already been saved as SCILAB variables using its sub function loadVariables(flashNumber). The function parameter "flashNumber" determines the flash to be loaded. Figure 5.12 shows the script plotEFieldOfFlash(flashNumber, time1) and its sub functions in a block diagram. The sub functions, clipVariable(time1) clips the SCILAB variable according to the given time length, correlation() determines the cross correlation between strokes and plot() displays the waveform of the electric field and the cross correlation of the strokes. The sub function saveClippedVariables() saves the clipped strokes as SCILAB variables.

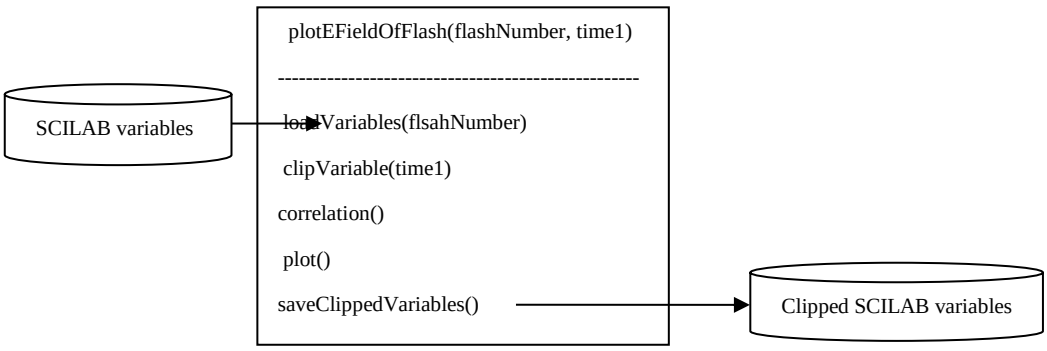

Figure 5.12: Script plotEFieldOfFlash() and its sub functions

The script **applyStatisticToData()** executes all mathematical, statistical calculations and plots the results. Figure 5.13 depicts the function applyStatisticToData() and its sub functions. It is apparent that the sub function getClippedStrokes() fetches the clipped SCILAB variables. The sub function chiSquare() calculates the chi square using the value of the electric field data of the strokes, while the sub function correlation() calculates the maximum of the cross correlation between the strokes. Furthermore, the sub function gMean() calculates the mean values with the results of the chi squares and the cross correlation and saves the results. The sub function plotEval() is responsible for plotting the diagrams of the results.

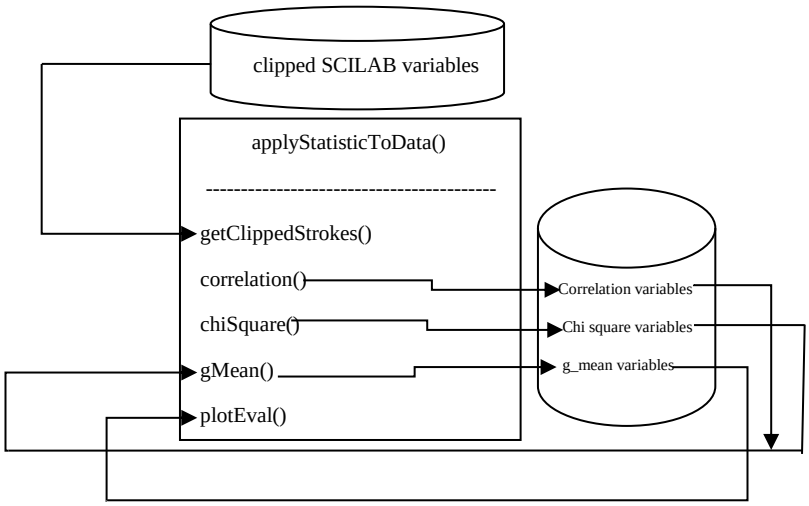

Figure 5.13: Script applyStatisticToData () and its sub functions

5.4 Data preparation

The electric field data of the strokes are loaded from the binary files and each stroke is clipped 30 µs prior to the striking time. With this value, the whole discharge process can be captured from the beginning. The complete time window is 1000 µs, which is then saved into the corresponding flash folders. Usually, the first 500 µs of a stroke are enough for the evaluation because they represent the significant characteristics of a discharge process, but a length of 1000 µs leaves more room to evaluate the data with different time durations. Figure 5.14 illustrates the first stroke N97F1 for a time window of 1000 µs. The vertical axis indicates the value of the electric field and the horizontal axis shows the time. The start time 138.85 ms and end time 139.85 ms of the first stoke are visible on the time axis.

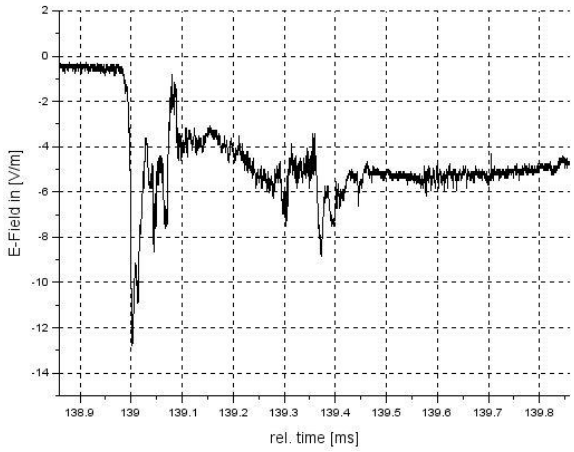

Figure 5.14: First stroke of flash N97 copied from the binary file for the time length of 1000 µs

In order to check the peak values and the alignment of the electric field, the strokes are plotted graphically and numerically again using the script plotEFieldOfFlash(flashNumber, time1). The electric field of the first stroke N97F1 and the subsequent strokes N97S1a and N97S1b of the flash N97 are illustrated in Figure 5.15.

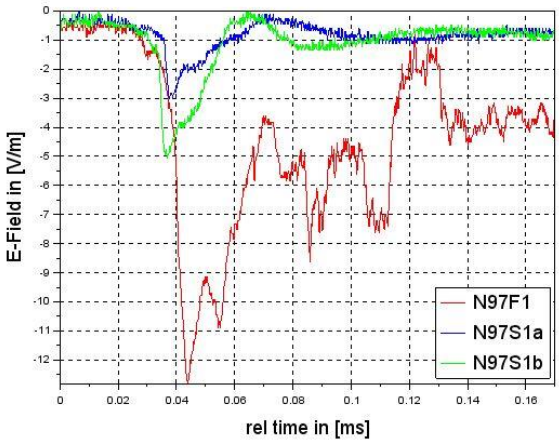

Figure 5.15: First and subsequent strokes of the flash N97

Looking at figure 5.15, it can be noted that the peak values of the electric fields of the strokes are not the same N97F1= -12.830 V/m, N97S1a= -3.038 V/m, N97S1b= -5.063 V/m. In addition to the unequal peak values, a displacement between the peaks of the strokes and an offset in the waveforms of the electric field within the interval 0-30 µs could be observed. Therefore, the following operations will be applied to the strokes:

- normalization of the peaks of the strokes
- fixing the alignment of the peaks of the strokes
- offset compensation

5.4.1 Normalization of peak to value one

In this thesis, the chi square differentiates each sample of two waveforms by the subtraction. Since the comparison of the waveform of the electric fields is of interest, not the peak value, that is why when the peaks have different values, they will bias the result of the chi square distribution. Because of this, the dependence on the peak value must be eliminated, so that it does not have any influence on our calculation. In order to get rid of this dependency, the strokes are normalized by their own maximum value, so the peaks of all strokes have value "1". Figure 5.17 represents the waveforms of the strokes of the flash N97 with the normalized peak values.

5.4.2 Fixing alignment of strokes

The displacement of the peaks of the waveforms can also affect the determination of the similarity of the waveforms. When the peaks of two waveforms at the same point of the horizontal axis are subtracted, then the subtraction produces a higher result if the peaks are not aligned together. That also causes an additional displacement in the curve of the cross correlation, see Figure 5.16. In order to avoid this type of error, the peaks of the strokes need be aligned at the same point. The waveforms of the strokes of each flash are shortened so long until their peaks align at the same point. In Figure 5.17, the strokes of the flash N97 are illustrated with the correct alignment.

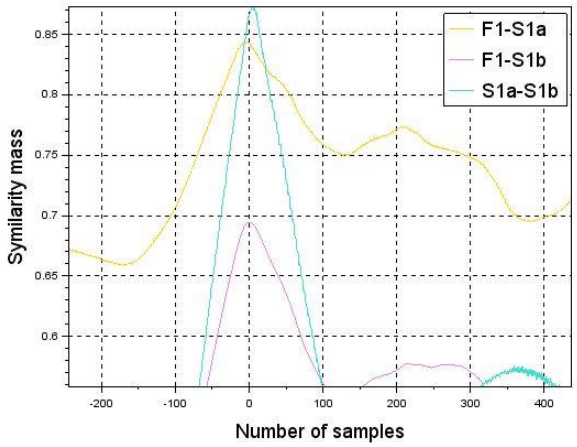

Figure 5.16: The displacement of the peaks of the strokes of the flash N97 in the cross correlation diagram without the same alignment

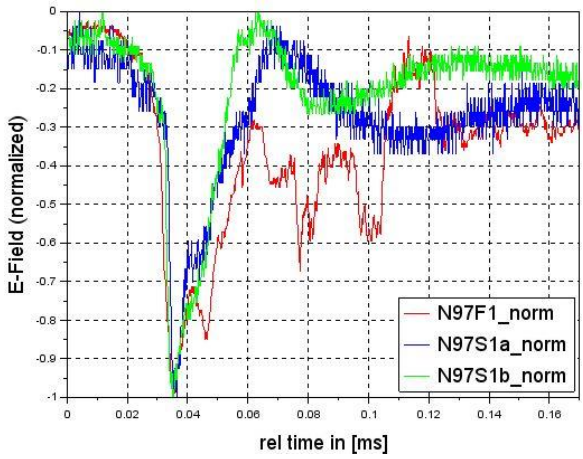

Figure 5.17: The correct alignment of the peaks of the Strokes of the flash N97

Figure 5.18.a illustrates the chi squares and the maximum of the cross correlation of the flash N97 with the normalized peaks and correct alignment, while the results with the un-normalized and shifted peak appear in Figure 5.18.b. The chi squares with the normalized peaks in Figure 5.18.a exhibit a considerable smaller value compared to chi squares with the un-normalized peaks.

```
The size of N97F1: 1 4001
The size of N97S1a: 1 4001
The size of N97S1a: 1 4001

The peak value of the E-Field of N97F1: -1.000000
The peak value of the E-Field of N97S1a: -1.000000
The peak value of the E-Field of N97S1a: -1.000000

The Chi Square distribution between N97F1-N97S1a: 0.040068
The Chi Square distribution between N97F1-N97S2a: 0.076857
The Chi Square distribution between N97S1a-N97S1a: 0.011847

The cross-corellation mass between N97F1-N97S1a: 0.937085
The cross-corellation mass between N97F1-N97S1a: 0.873798
The cross-corellation mass between N97S1a-N97S1b: 0.938900
```

5.18.a: Normalized peak values

```
The size of N97F1: 1 4001
The size of N97S1a: 1 4001
The size of N97S1a: 1 4001

The peak value of the E-Field of N97F1: -12.825821
The peak value of the E-Field of N97S1a: -3.037694
The peak value of the E-Field of N97S1a: -5.062824

The Chi Square distribution between N97F1-N97S1a: 20.555704
The Chi Square distribution between N97F1-N97S2a: 20.298814
The Chi Square distribution between N97S1a-N97S1a: 0.118701

The cross-corellation mass between N97F1-N97S1a: 0.937085
The cross-corellation mass between N97F1-N97S1a: 0.873798
The cross-corellation mass between N97S1a-N97S1b: 0.938900
```

5.18.b: Un-normalized peak values

Figure 5.18: Distinction of the chi squares with the normalized and un-normalized peak values of the electric fields of the strokes of the flash N97

5.4.3 Offset compensation

The motivation for the offset compensation in the waveform of the strokes is also to reduce errors in the calculation. For the offset compensation, first, the mean value of the electric field of each stroke for the interval 0 to 20 µs is calculated. Afterwards, this value is subtracted from the whole electric

field data of the corresponding stroke. Figure 5.19 shows the waveforms of the electric field of the first stroke N122F2 and its subsequent strokes N122S2a, b, c of the flash N122 without offset compensation. The waveforms of the electric fields exhibit an offset that is apparent within the interval 0 to 0.035 ms and whose value ranges from -0.05 V/m to -0.15 V/m. After the offset compensation, all curves are moved close to zero of vertical axis, see Figure 5.20.

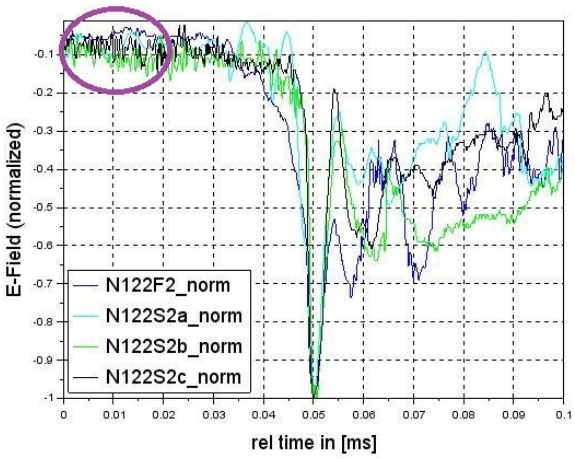

Figure 5.19: First stroke N122F2 and subsequent strokes N122S2a, b, c before offset the compensation

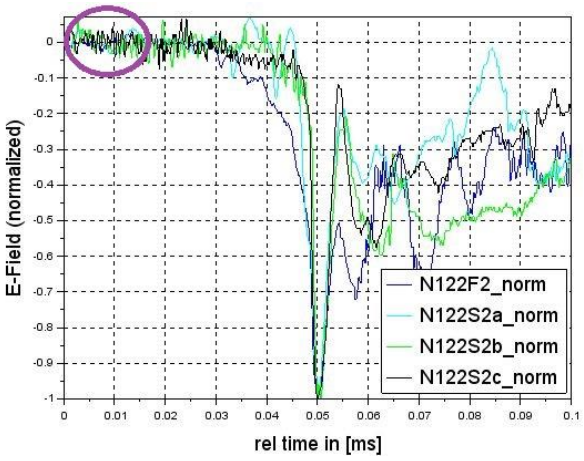

Figure 5.20: First strokes N122F2 and subsequent strokes N122S2a, b, c after the offset compensation

5.5 Selection of data for the evaluation

Throughout the investigation, some strokes of the flashes turned out as unusable for the evaluation. The reasons for this are:

- strokes with saturated electric field

- strokes, which have double peaks in their waveform

Sometimes the electric field of a lightning stroke can have more than one peak within a discharge process. Those peaks are separated by a time of about 200 to 400 µs and the second peak has often a higher value than the first one. These types of stroke do not fit to the approach of this master's thesis and are discarded. The reason is the normalization of the first peak, because as soon as a longer time length for the evaluation is selected, the first peak of the electric field obtains its original value, while the posterior peak is normalized to value one because of being the maximum value. This will bias the value of the chi square when two waveforms will be compared to each other. In Figure 5.21, the strokes N104F1 and N104F2 are respectively represented in red and blue. Apparently, the peak of the stroke N104F2 is around 0.04 ms, whereas the stroke N104F1 has multiple peak; the first is at 0.04 ms and the other peaks are at 0.456, 0.598 and 0.71 ms.

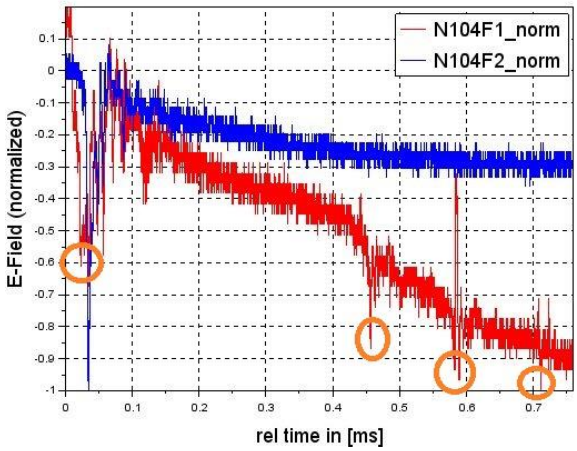

Figure 5.21: Double peaks of the stroke N104F1

Further, there are strokes containing two peaks which are very close to each other (between 2 to 3 µs, see Figure 5.22). In this case, the first peak from the left (encircled in orange color) will be considered for the evaluation.

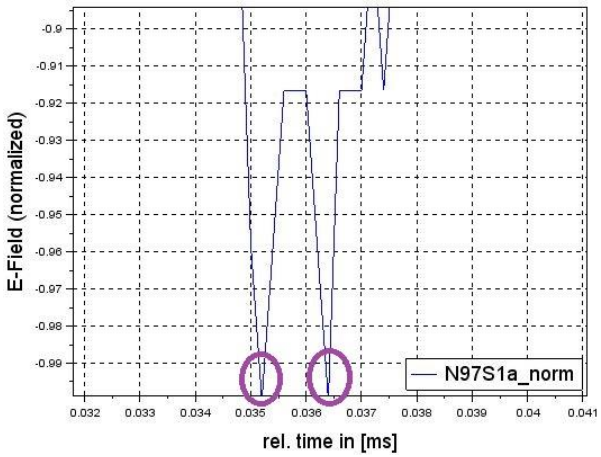

Figure 5.22: Double peaks of subsequent stroke N97S1a

The strokes, which contain saturated electric fields are also not used for the evaluation and discarded. The reason for the saturation may be that the peak of the electric field exceeded the detector's capacity range during the detection period or noise, precipitation.

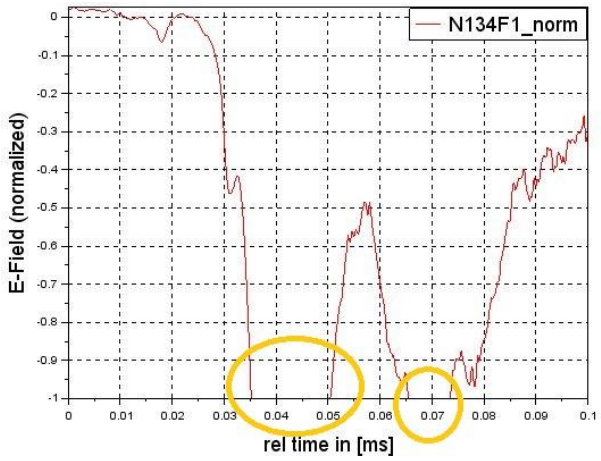

Figure 5.23: Saturated electric field of first stroke N134F1

Calculating the chi square and cross correlation of those strokes with the undefined peaks can forcibly falsify the results because the peak values are then assigned to the strokes by the analysis software SCILAB. In Figure 5.23, the saturated electric field of the first stroke N134F1 of the flash N134 is depicted. The beginning and the end of the discharge can be seen in the figure. However, the tip of the peaks between (0.035 and 0.051 ms) and (0.065 and 0.074 ms) of the time axis is not visible.

The flashes with the discarded strokes are listed in Table 5.2. The column on the left shows the flashes, whose strokes have turned out as unfit for the evaluation during the investigation of the flashes. The middle column depicts, whether a stroke is excluded from the calculation of the chi square between

the first versus first, first versus subsequent or subsequent versus subsequent strokes. The column on the right represents the discarded strokes.

Table 5.2: List of flashes with discarded strokes

Flash number	Distribution between first versus first, first versus subsequent, subsequent versus subsequent strokes	Discarded strokes
N104	First stroke versus first strokes	N104F1
N122	First versus first, subsequent versus subsequent strokes	N122F3, N122S2a, b, N122S3a
N124	First stroke versus first, first versus subsequent strokes	N124F3
N128	First stroke versus first, first versus subsequent strokes	N128F1
N134	First stroke versus first, first versus subsequent strokes	N134F1
N171	First stroke versus first strokes	N175F2
N175	First stroke versus first, first versus subsequent strokes	N175F2
N221	First versus subsequent strokes, subsequent versus subsequent strokes	N221S1e
N229	First stroke versus first, first versus subsequent strokes	N229F1, N229F2
N280	First versus subsequent strokes, subsequent versus subsequent strokes	N280S1d
N322	First versus first strokes	N322F2

6. Results

This chapter discusses the results of the comparisons accomplished by calculating the chi squares and cross correlations. Section 6.1 outlines the results of the comparisons between the first versus first, first versus subsequent, and subsequent versus subsequent strokes separately, whereas Section 6.2 presents the overall results of the previous section and validates these results relating to the hypothesis of this master's thesis.

6.1 Results of the chi squares and cross correlation between strokes

After discarding the unqualified strokes, the evaluation is executed using the data. The criteria for discarding the strokes were discussed in Section 5.5. The evaluation of the first versus subsequent, and subsequent versus subsequent strokes of a flash always involves the strokes from the same channel. Further, the first stroke of the same flash of a channel is compared to the first strokes of other channels. The electric fields of the strokes are evaluated for five different time lengths which are 50, 100, 300, 400, and 600 μs. These time lengths are highlighted along the time axis in Figure 6.1 respectively in green, cyan, orange, black, and violet. In this section, only the results for the time length of 100 μs are visualized. The results of the other time lengths will be analyzed and presented in Section 6.2. 45 flashes containing 117 first strokes were involved in the calculation of 72 chi squares between the first strokes. Figures 6.2 and 6.3 illustrate the histograms of the chi squares and cross correlations between the first strokes.

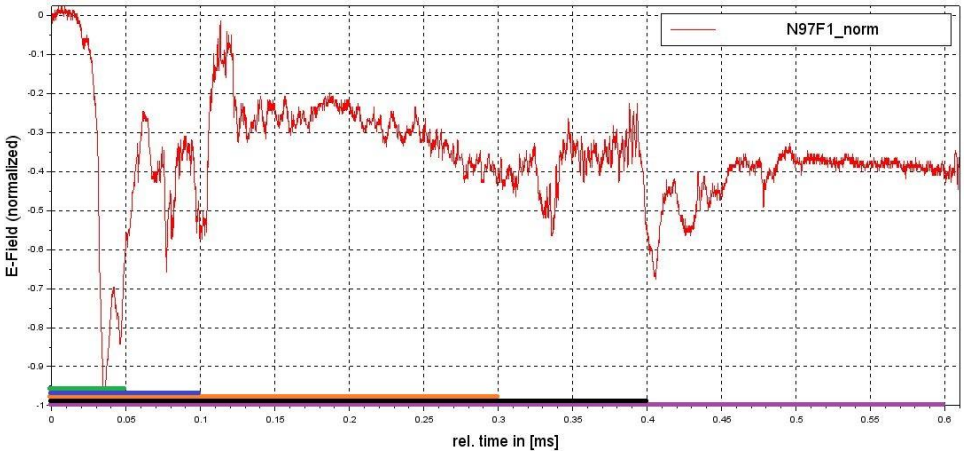

Figure 6.1: The time lengths for the evaluation are drawn along the time axis in five different colors

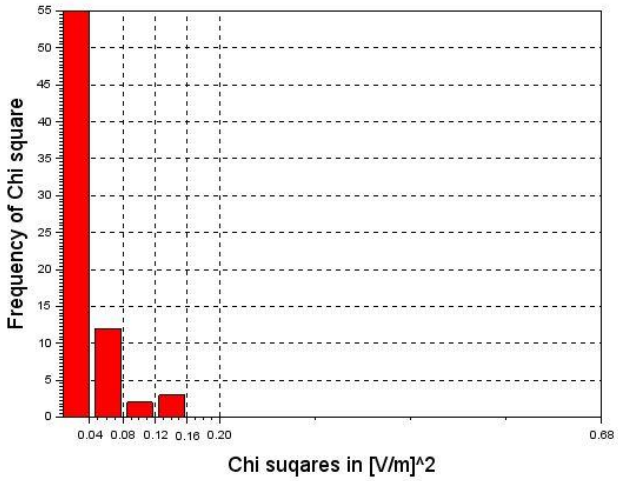

Figure 6.2: Chi squares between the first strokes of different channels for the time duration of 100 µs

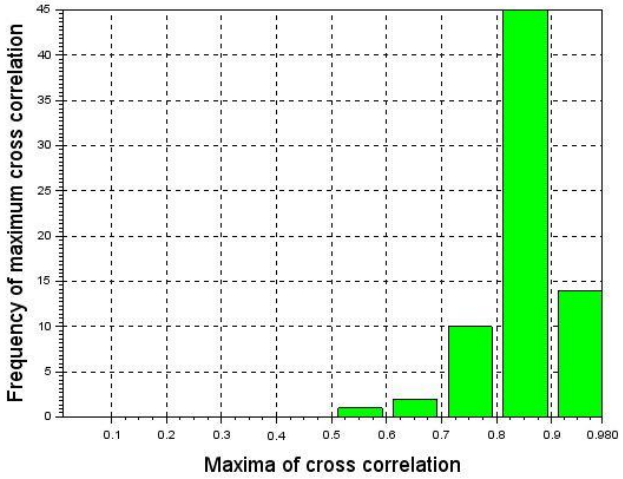

Figure 6.3: Maxima of the cross correlation between the first strokes of different channels for the time duration of 100 µs

56 first strokes and 149 subsequent strokes of 53 flashes were taken into account for the calculation of 149 chi squares between the first and subsequent strokes of the same channel. Figures 6.4, 6.5 respectively show the histograms of the chi squares and maxima of the cross correlation between the first and subsequent strokes.

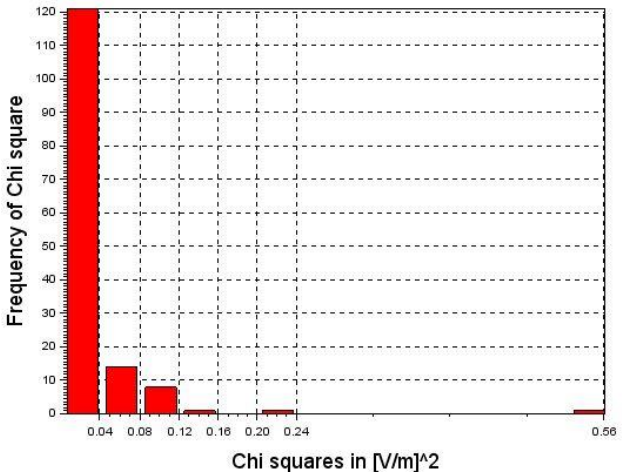

Figure 6.4: Chi squares between the first and subsequent strokes of the same channel for the time duration of 100 µs

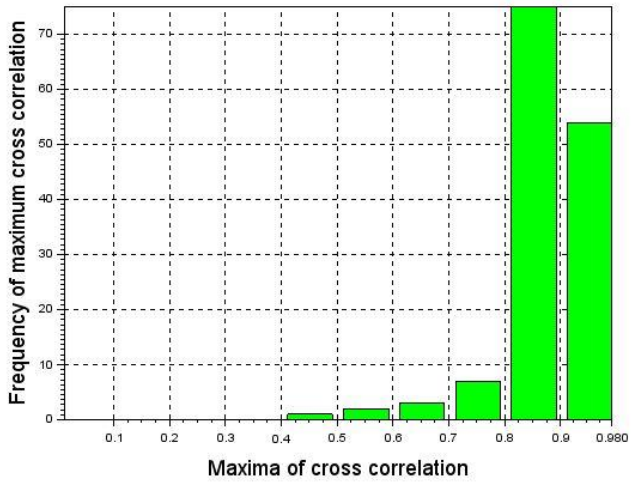

Figure 6.5: Maxima of the cross correlation between the first and subsequent strokes of the same channel for the time duration of 100 µs

133 subsequent strokes of 35 flashes were selected for the calculation of the chi square and the cross correlation between the subsequent strokes and yielded 95 chi squares and cross correlations. Figures 6.6 and 6.7 illustrate the histograms of the results.

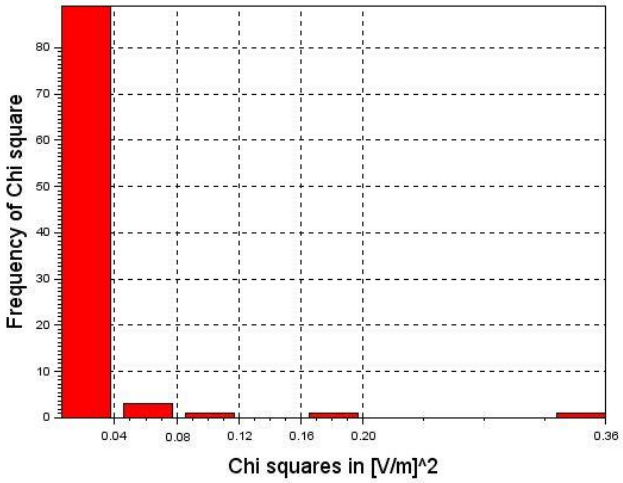

Figure 6.6: Chi squares between the subsequent strokes of the same channel for the time duration of 100 µs

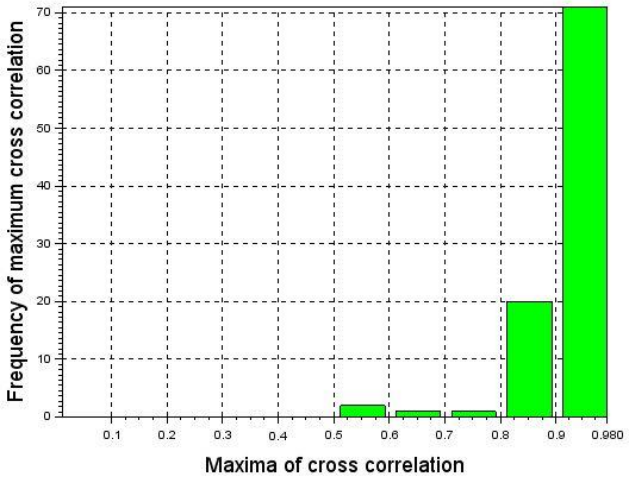

Figure 6.7: Maxima of the cross correlation between the subsequent strokes of the same channel for the time duration of 100 µs

6.2 Overall results and validation of the results regarding the hypothesis

The calculation of the mean chi square and the mean of the maxima of the cross correlation were performed under considering the time duration and the detection range at which the strokes were detected. Consequently, the dependence of the results on time duration and detection range can be explored. Therefore, the mean of the chi square was calculated:

- Without considering the detection range and involving all flashes
- Separating the detection ranges in two intervals, 15 to 30.9 km and 31 to 60 km.

78 first strokes of 31 flashes and 40 first strokes of 15 flashes were detected respectively within the detection range of 15 to 30.9 and 31 to 65km. The corresponding number of the chi squares between the first strokes of these two groups are 47 and 25.

40 first and 102 subsequent stokes of 36 flashes detected within 15 to 30.9 km yielded 102 chi squares between the first and subsequent strokes. 19 first and 47 subsequent strokes of 19 flashes detected within 31 to 65 km resulting in 47 chi squares between the first and subsequent strokes.

90 subsequent strokes of 24 flashes detected within 15 to 30.9 km and 43 subsequent strokes of 13 flashes detected within 31 to 65 km output 65 and 30 chi squares.

The mean chi square and the mean cross correlation without considering the detection range are presented in Figures 6.8 and 6.9 for the time duration of 50, 100, 300, 400, and 600 µs.

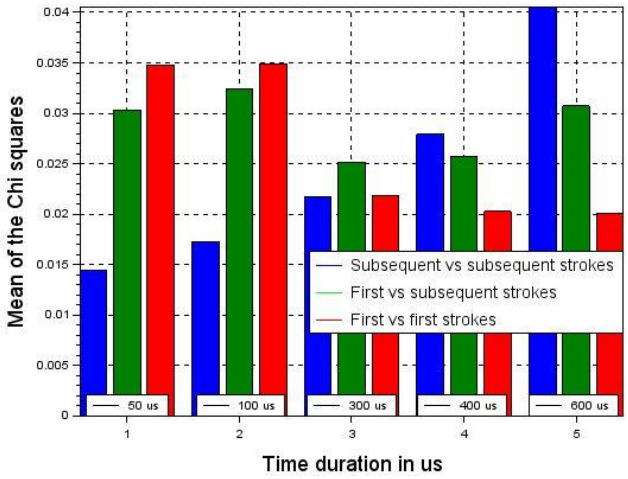

Figure 6.8: Mean chi squares between the subsequent, the first and subsequent and between the first strokes without considering the detection range

As evident in Figure 6.8, the mean chi square between the subsequent strokes (blue bars) is lower compared to the mean chi square between the first and subsequent strokes (green bars), furthermore, the mean chi square between the first and subsequent strokes (green bars) is lower compared to the mean chi square between the first strokes of different channels (red bars) for the time duration of 50 and 100 us. Thereby, they meet the expectation of the hypothesis.

Figure 6.9 illustrates the mean cross correlation, which fulfills the hypothesis for all time periods. However, from the time duration of 100 us the values become smaller than 0.90, which indicates a poor similarity. Because of the considerable similarity between the subsequent strokes, their mean cross correlation has a higher value (blue bars) compared to the mean cross correlation between the first and subsequent strokes (green bars). Moreover, the mean cross correlation between the first and subsequent strokes has a higher value compared to the mean cross correlation between the first strokes (red bars). The closer the mean cross correlation to one the better agreement between the waveforms in the corresponding lag.

As can be seen in Figures 6.8, the analysis is more correct for the time durations of 50 and 100 us. The possible reason may be the measurement error of the electric field. Probably, with increasing time duration, the electric field of the return stroke decayed. As a result, the similarity between the waveforms of the electric fields in some cases is distorted.

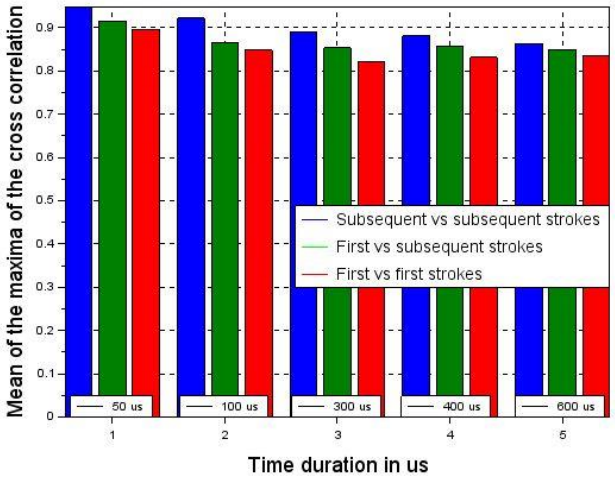

Figure 6.9: Mean cross correlation between the subsequent, the first and subsequent, and between the first strokes without considering the detection range

In Figures 6.10 and 6.11, the mean chi squares and the mean cross correlation of the strokes detected at a distance within 15 to 30.9 km are illustrated for five different time durations. It is apparent that the mean chi square and the mean cross correlation satisfies the hypothesis for the time durations of 50, 100 and for 300 µs.

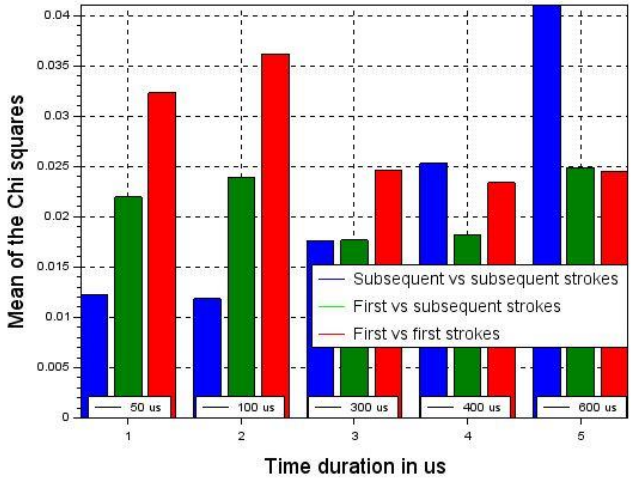

Figure 6.10: Mean chi squares between the subsequent, the first and subsequent and between the first strokes for the detection range of 15 to 30.9 km

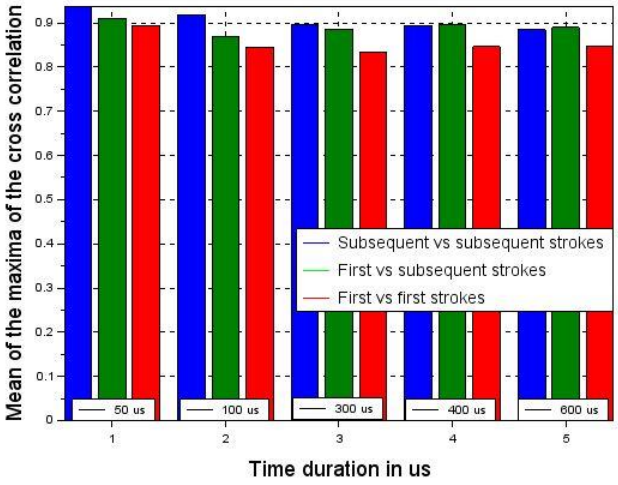

Figure 6.11: Mean cross correlation between the subsequent, the first and subsequent, and between the first strokes for the detection range of 15 to 30.9 km

Figures 6.12 and 6.13 present the mean of the chi squares and the mean cross correlation of the strokes detected at a distance within 31 to 60 km. Noteworthy is that the results of the mean chi squares do not follow the expectation of the hypothesis for any time duration. Presumably, due to a long distance between the LLS and the GSP of the strokes, the propagation of the electric field of the strokes was obstructed and attenuated in the environment; led to measurement errors. That is why the mean chi square did not align with the expectation of the hypothesis.
However, the mean cross correlation satisfies the hypothesis for the time duration of 50 and 100 µs. Unlike the time duration of 50 µs, the values for time duration of 100 µs are smaller.

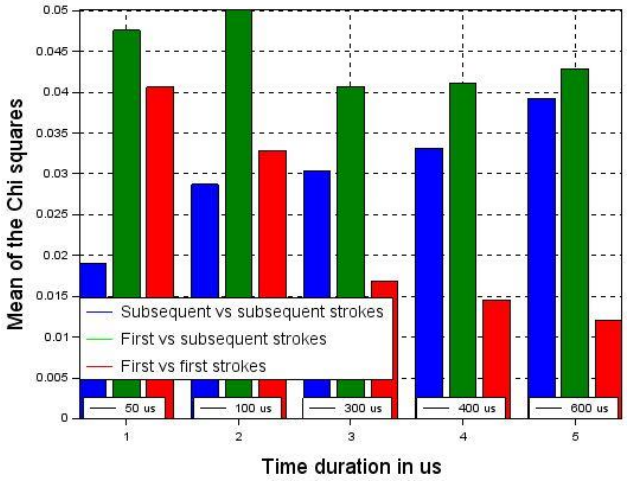

Figure 6.12. Mean chi squares between the subsequent, the first and subsequent, and between the first strokes for the detection range of 31 to 60 km

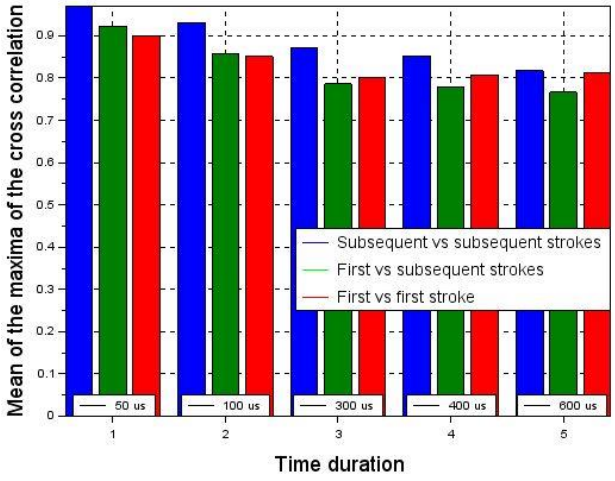

Figure 6.13: Mean cross correlation between the subsequent, the first and subsequent, and between the first strokes for the detection range of 31 to 60 km

An evaluation of the waveform of the electric field between the subsequent strokes from different GSPs of a flash is conducted as well. Eleven subsequent strokes of four flashes from different GSPs output seven chi squares and cross correlations. As can be seen in Figure 6.14, the mean chi square between the subsequent strokes from the same channel (blue bar) has a lower value compared to the green bar that represents the mean chi square between the subsequent strokes from different GSPs. In Figure 6.15, it is also noticeable that the mean cross correlation between the subsequent strokes from the same channel is similar compared to the mean cross correlation between the subsequent strokes from different channels.

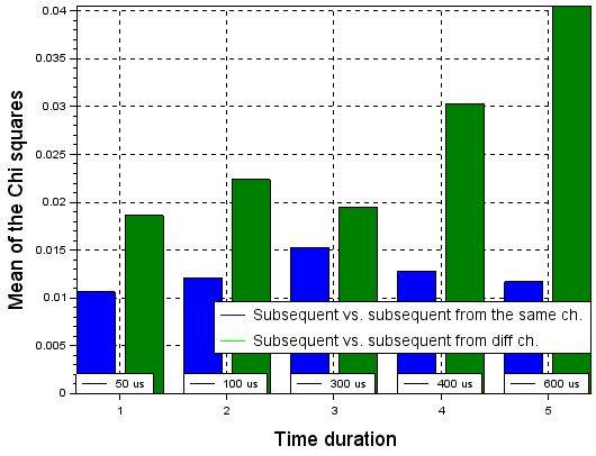

Figure 6.14: Mean chi square between the subsequent strokes from the same and different channel

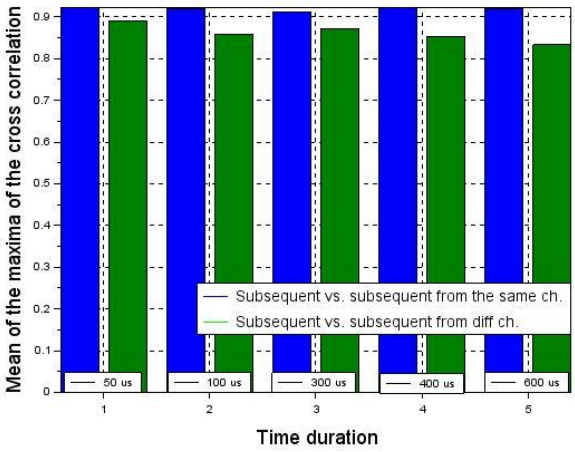

Figure 6.15: Mean of the maxima of the cross correlation between the subsequent strokes from the same and different channel

7. Discussion and conclusion

72 flashes containing 298 strokes ware qualified for the evaluation of the hypothesis of the master's thesis. The evaluation was accomplished based on the calculation of the chi square. The cross correlation was applied not only to get the quantitative values of the comparisons but also to verify, in which lag of the time axis the waveforms have a higher similarity. The mean chi square and the mean cross correlation were calculated without considering the detection range, which involved all strokes. In the further calculation, the strokes were separated based on their detection range (15 to 30.9 km) and (31 to 60 km). Each of the calculations mentioned above was performed for the time duration of 50, 100, 300, 400 and 600 us. The evaluation was performed:

- between the first strokes from different GSPs of the same flash
- between the first and subsequent strokes of the same channel
- between the subsequent strokes of the same channel
- between the subsequent strokes from different channel of a flash

The values of the chi squares and cross correlations were affected by the imprecise alignment of the first peaks of the strokes because the peaks of some strokes of a flash could not be aligned exactly in the same point of time.

The evaluation of these four groups of the strokes (first versus first, first versus subsequent and subsequent versus subsequent, subsequent versus subsequent from different GSPs) could not be conducted with the same number of strokes.

It occurred frequently that not all strokes of a flash were found within the same interval of the detection range, e.g. four of the five strokes of a flash were detected within the detection range of 15 to 30.9 km and the remaining at a distance of 35 km. In this case, this stroke was added to the detection range group of 31 to 65 km.

In the course of the calculation, it was revealed that the mean chi squares without considering the detection range meets the expectation of the hypothesis for the time durations of 50 and 100 µs, while the mean cross correlation meets the hypothesis for all time duration.

In case of the detection range of 15 to 30.9 km, the mean chi squares and mean cross correlation conform to the hypothesis for the time durations of 50, 100 and 300 us.

The mean chi squares of the strokes located within the detection range of 31 to 60 km do not meet the hypothesis for any of the time duration. However, the mean cross correlation fulfills the hypothesis for the time duration of 50 and 100 µs.

Throughout the analysis, it can be stated that the hypothesis of the master's thesis is correct for a shorter time duration of 50 and 100 us and a detection range between 15 to 30.9 km. For a longer time

duration and detection range, e.g. 400 us and 50 km, the hypothesis is hard to apply because the electric fields of the strokes depart from each other, besides they attenuate in the environment by obstacles and precipitation. Additionally, the precession of the measurement devices and distance between the device and the striking point also play an important role.

For the evaluation of the waveform of the electric field between the subsequent strokes from different GSPs, only four flashes with eleven strokes were considered. Because there were not enough flashes, which had multiple subsequent strokes at multiple GSPs. It will be interesting to examine flashes with multiple subsequent strokes at multiple GSPs.

In the evaluation of the subsequent strokes from the same channel, the first subsequent stroke was always compared to further subsequent strokes. An analysis of the differences between the second subsequent stroke and further subsequent strokes from the same channel was not done. It might be a possible future work to examine the similarities between the second subsequent stroke and its following strokes which struck later and so on.

An attempt was made to order the strokes by the detection range in 10 km steps in ascending order, so, 15, 25, 35, 45, 55, 65 km. Since there were not enough strokes for all of these detection ranges, the strokes were divided into two detection range groups only. With a larger data set, it might be interesting in the future to analyze strokes for more detection ranges.

Bibliography

Baudin, R.: Run time comparison of MATLAB, Scilab and GNU Octave on various benchmark programs, July 2016.

Becke, D. C. and Serpa, A. L.: Comparison of the main features of SCILAB, OCTAVE and MATLAB for some optimization and control problems, in: XXIII Congress of Scientific Initiation of Unicamp, Brazil 2015.

G. Diendorfer, W. Schulz, OVE-ALDIS, Vienna, Austria; C. Cummins, Univ. of Arizona., Tucson, USA; V. Rakov, Univ. of Florida, Gainesville, FL, USA; M. Bernardi, CESI, Milano, Italy; F. De La Rosa, Twiacs, St. Louis, USA; B. Hermoso, Univ. of Navarra, Pamplona, Spain; A. M. Hussein, Reyerson Univ., Toranto, Canada; T. Kawamura, Shibura Inst. of Technology, Tokyo, Japan; F. Rachidi, EPFL, Lausanne, Switzerland and H. Torres, Univ. Nacional de Colombia, Bogota, Colombia: Cloud-to Ground Lightning Parameters derived from Lightning Location Systems, in: 2009 CIGRE SC C4 2009 Kushiro Colloquium The Effects of System Performance.

Bouquegneau, C.: History of Lightning, in: 2011 7th Asia Pacific Int. Conf. Light., pp. 571-574, Nov 2011.

Cummins, K. L., and Murphy, M. J.: An Overview of Lightning Locating Systems: History, Techniques, and Data Uses, With an In-Depth Look at the U.S. NLDN, in: IEEE Trans. Electromagn. Compat., vol 51. no.3, pp. 499-518, 2009.

Diendorfer, G., Schulz, W., and Scherney C.: AREAS OF INCREASED LIGHTNING FLASH DENSITY ON MOUNTAIN TOPS, in: Austrian Lightning Detection & Information System, June 1997, pp. 1-3.

Diendorfer, G., Schulz, W.: ALDIS Austrian Lightning Detection and Information System 1992-2008, in: Elektrotechnik und Informationstechnik, vol. 125, no.5, pp. 209-213, May 2008.

Haight, F. A.:Handbook of the Poisson Distribution, in: Publication in Operation Research/ Operation Research Society of America, No. 11, John Wiley & Sons, New York, 1967.

George, P., Brayan, J., Wadsworth, G.: Introduction to Probability and Random Variables, in: MacGraw-Hill Series in Probability and Statistics. 7th printing edition, New York, 1960, pp.52.

Graham, B. L., Holle, R. L., and Lopez, R.: Lightning Detection and Data News, in: Fire Management Notes, vol.57, no.2, pp.4-11, 1997.

Hanke, J.: Calibration of the Recording of Far Field Radiated by Lightning Strikes to the Gaisberg Tower, in: Master's thesis, Vienna University of Technology, faculty for Electronic and Information Technology, institute for Energy Systems and electric Drives, E370, 2014.

Heidler, F., Zischank, W., Fliosowki, Z., Bouquegneau, C. and Mazzetti, C.: "29th international Conference on Lighting Protection Parameters of Lightning Current given in IEC 62305, Background, Experience and Outlook," Uppsala, Sweden, 2008.

Heikell, E. W. J.: SCILAB for Real Dummies, in: Introducing an Open-Source Alternative to Matlab, v1.0/SCILAB 5.3.2 (5.3.3), 2014, pp.10-23,

Holle, R. L.: Annual Rates of Lightning Fatalities by Country, in: In 20th International Lightning Detection Conference, 2008, p.14.

Beard, K. v. K. and Ochs, H. T.: Charging Mechanism in Clouds and Thunderstorms, in: The Earth's electric Environment, New York, National Academy Press, 1986, p. 263.

Koudelka, G., Egger, B., Jossekck, N., Deschamp, C., Crodell Grant, D., Foisy, R., Zee, W., Weiss, R., Kusching, A., Scholtz, A., and Keim, W.:TUGSAT-1/BRITE-Austria, in: The first Austrian nanosatellite, Acta Astronaut., vol. 64, no. 11-12, pp. 1144-1149, June 2009.

Krehbiel, P. R.: The electric Structure of Thunderstorms, in: The Earth's electric Environment, Washington D.C., National Academy Press, 1986, pp. 263.

Mazzoni, T.: Zeitreihenanylyse Wirtschaftswissenschaft, in: Skript, Fernuniversität in Hagen, 2010, pp. 12-16.

Papula, L.: Mathematik für Ingenieure und Naturwissenschaftler Band 3, in: 4. Auflage, Vieweg Verlag, 2001, pp614.

Rakov, V. A., Thottappillil, R. and Uman, M. A.: FIRST VS. SUBSEQUENT STROKE INTENSITY AND MULTIPLE CHANNEL TERMINATION IN COLOUD-TO-GROUND LIGHTNING, in: 21st ICLP International Conference on Lightning Protection, Berlin, Germany, September 21-25, 1992.

Rakov, V. A. and Uman, M. A.: LIGHTNING Physics and Effects, in: First edition, Cambridge University Press, 2003, pp. 44-45,687.

Schulz, W., Diendorfer, G., Pedeboy, S. and Roel Poleman, D.: The Eurpean lightning location system EUCLID Part1, in: Performance analysis and validation

Smorgonskiy, A., Rachidi, F., Rubinstein, M. and Diendorfer, G.: On the Relation between Lightning Flsah Density and Terrain Elevation, in: 2013 International Symposium on Lightning Protection (XII-SIPDA), Belo Horizonte, Brazil, October 7-11,2013.

Schulz, W. (ALDIS), Verginer, C. (TU Graz), Pichler, H. (ALDIS), Diendorfer, G. (ALDIS), and Pack, S. (TU Graz): VALIDATION OF THE AUSTRIAN LIGHTNING LOCATION SYSTEMS FOR NEGATIVE FLASHES, in: CIGRE C4 Colloquium on Power Quality and Lightning, Sarajevo, Bosnia and Herzegovina, 13-16 May, 2012, pp.2

Vergeiner, C., Pack, S., Schulz, W., and Diendorfer, G.: Negative CG Lightning in the Alpine Region, in: 2016 CIGRE C4 International Colloquium on EMC, Lightning and Power Quality Consideration for Renewable Energy Systems, 2016, pp.1-5.

Weyerhäuser, K.: Faltung und Korrelation kontinuierlicher Signale, in: Seminar, Digitale Signalverarbeitung, Institut für Integrierte Naturwissenschaften Abteilung Physik, Universität Koblenz, 2005, pp. 9-12.

Internet references

[1] https://www.aldis.at/blitzstatistik/tabellen/, 16.11.16

[2] http://www.aldis.at/

[3] www.bmi.gv.at/cms/BMI_OeffentlicheSicherheit/2009/07_08/files/Blitzschuzt.pdf, “Gefahr von Oben”.

[4] https://de.mathworks.com/help/signal/examples/measuring-signal-simila, 10.09.17

[5] https://explorable.com/chi-square-test, 28.09.17

[6] www.heikel.fi/downloads/SCILAB.ppt, 21.09.17

[7]https://www.revolvy.com/main/index.php?s=Comparison%20of%20computer%20algebra%20systems&item_type=topic, 21.09.17

[8] https://onlinecourses.science.psu.edu/stat500/node/22, 23.09.17

[9] https://www.umass.edu/wsp/resources/poisson/, 24.09.17

[10] http://www.probabilityformula.org/hypergeometric-distribution.html, 24.12.17

[11] https://www3.nd.edu/~rwilliam/stats1/x21.pdf, 27.09.17

[12] http://www.investopedia.com/terms/n/normaldistribution.asp 27.09.17

[13] http://people.stern.nyu.edu/adamodar/New_Home_Page/StatFile/statdistns.htm, 21.09.17

[14] http://www.statisticssolutions.com/correlation-pearson-kendall-spearman/, 24.01.18

[15] https://help.SCILAB.org/doc/5.3.3/en_US/section_0e2c3baade72c97c1c28ae3cb0c431fc.html, 12.10.17

[16] http://midas-player.software.informer.com/2.1/, 20.09.17

[17 neu] http://www.xcitex.com

[18] https://www.SCILAB.org/SCILAB/about, 24.01.18

[19] https://help.SCILAB.org/doc/5.5.2/en_US/color_list.html, 10.11.17

[20] http://www.openeering.com/sites/default/files/LHY_Tutorial_Gui.pdf 12.10.17

[21] https://wiki.SCILAB.org/howto/guicontrol, 12.10.17

[22] http://profs.scienze.univr.it/~caliari/pdf/octave.pdf, 10.12.17

[23] http://users.uom.gr/~samaras/pdf/C53.pdf, 10.12.17

[24] http://ams.com/eng/Products/Wireless-Connectivity/Wireless-Sensor-Connectivity/AS3935, 18.02.18